JOURNAL OF MATERIALS SCIENCE 20 (1985) 761–796

Review
Some transport properties of transition metal films

M. A. ANGADI
Department of Physics, University of the West Indies, St. Augustine, Trinidad, West Indies

Recent experimental measurements reported on the electrical resistivity, temperature coefficient of resistance and thermoelectric power of nineteen transition metal films have been reviewed. All the theoretical models proposed so far to analyse these experimental results have been briefly summarized. Some suggestions for further experimental study on transition metal films are outlined.

1. Introduction

The peculiar structure and conduction phenomena of thin films have given them great technological potential, especially for microelectronics and optical devices. Considerable reduction in space and material consumption have greatly minimized the cost of these thin film devices. The low cost, thermal and time stability, have made thin film devices very popular and useful compared to other devices. Although many semiconductor materials are used in thin film form, the utility of a host of metallic substances is yet to be explored. Among metallic substances, transition metals find extensive applications in the preparation of very large area, light weight and inexpensive electronically active and passive devices. Transition metal films (e.g. chromium, tantalum, manganese, tungsten and titanium) find frequent use as thin film resistor elements because of their unusually high resistivity and low temperature coefficient of resistance (TCR). The oxides of some of these transition metals (e.g. Ta_2O_5 and TiO_2) are used as high-permittivity dielectric material in the fabrication of thin film capacitors. Many transition metals are ferromagnetic materials (e.g. iron, cobalt and nickel) and have plenty of applications in the microelectronics industry. Refractory metals like tungsten, molybdenum and tantalum are used as source materials for thermal evaporation because of their high melting points. In view of these wide ranging applications the preparation and properties of transition metal films have become the subject of broad investigation for nearly the last two decades.

The physics of these transition metals is very complex in bulk materials and is further complicated in thin films because of the size effect and grain boundary scattering of conduction electrons. In general, the density of states in metals follows, to a good approximation, the free electron model. However, the transition metals cannot be represented by a free electron model because of the manner in which the electrons of these elements are distributed in their atomic orbits. The transition metals are characterized by the filling of the 4s shells before completely filling the 3d shell. In solids, where the discrete levels split into bands, there is an energy overlap between the 3d and 4s bands. The unusual physical properties of transition metals are mainly because of the scattering from the 4s to the 3d band. Since the 3d band is nearly full, its electrons contribute very little to conduction so that the conductivity of these materials is mainly due to the 4s electrons. At higher temperatures, the probability of scattering into the 3d band is considerably enhanced, but because not many states are available such events tend to be comparatively few in number. This extra s–d interaction will therefore lead to a higher electrical resistivity and small TCR for the transition metals compared to other metallic substances. It is reported [1] that over a small temperature range these metals and their alloys have nearly zero TCR. These rather unusual and

0022–2461/85 $03.00 + .12 © *1985 Chapman and Hall Ltd.*

interesting transport properties of transition metals render them suitable for many applications in electronics.

During the last decade or so, several excellent reviews [1–9] have been published on the electron transport in thin films. Considerable experimental and theoretical work has been published in recent years on the transport properties of transition metal films. It is appropriate at this juncture to review the published work in this field.

In this review, we consider only three transport properties, namely: (i) electrical resistivity, (ii) temperature coefficient of resistance (TCR) and (iii) thermoelectric power (TEP) of transition metal films. We review these experimental results in discontinuous and continuous transition metal films. The discussion of theoretical models and experimental results will be confined to polycrystalline and single crystal films, and readers are referred to a recent review by Bennet and Wright [5] for amorphous transition metal films. The scope of this review is limited to the published experimental work covering a period of about twenty years from 1963 to 1983. Earlier published work has already been reviewed by Maissel [1], Chopra [2], Hill [4] and Coutts [9].

Of late, considerable progress has been made in developing new theoretical models to account for the vast amount of experimental data published on thin metallic films. In the second section of this article, we briefly review various theoretical models used to analyse experimental results in discontinuous and continuous metal films. In the third section, we review the experimental results on nineteen transition metal films. Finally, some suggestions for further experimental work are briefly outlined which may help to resolve some of the anomalies and disagreements reported by different workers.

2. Theoretical development

2.1. Electrical conduction

2.1.1. Conduction in bulk metals

The free electron model due to Sommerfeld [10] assumes that the electrons of unfilled shells, i.e. the conduction electrons, are not deflected by the ion cores that are arranged on a periodic lattice. This gas of non-interacting electrons is able to propagate freely in a periodic lattice. A conduction electron is scattered randomly and infrequently only by other conduction electrons. The average distance travelled between such electron–electron collisions is called the mean free path (m.f.p.) of the conduction electrons, l_0. It is these conduction electrons that wholly contribute to the electron transport properties in metals.

However, that the electrons are fully free in a periodic lattice is only an ideal concept. The lattice cores are thermally vibrating about their mean positions to result in a phonon wave in the lattice. The phonon wave along with impurities and defects deviate the periodic potentials and thus serve as scattering centres for electrons. The total resistivity of the metal is due to this scattering of conduction electrons. This fact is incorporated in Mattheissen's rule, which defines a single relaxation time (time taken for the electron to travel distance l_0) τ_b in terms of the individual relaxation times of the various sources of electron scattering in the bulk material as [11]

$$\frac{1}{\tau_b} = \frac{1}{\tau_{lat}} + \frac{1}{\tau_{imp}} + \frac{1}{\tau_{def}} \qquad (1)$$

where τ_{lat}, τ_{imp}, τ_{def} are relaxation times due to lattice, impurity and defects, respectively. τ_{lat} due to phonons is predominant at high temperature. As temperature decreases only τ_{imp} and τ_{def} persist. Since resistivity is proportional to the reciprocal of the relaxation time, the individual resistivities can thus be added, namely

$$\rho_b = \rho_{lat} + \rho_{imp} + \rho_{def} \qquad (2)$$

Many deviations from Mattheissen's rule have in fact been observed in metals. It is important to note that the validity of this rule is based on the assumption of a constant relaxation time, and this is not always feasible.

2.1.2. Conduction in thin metal films

The real metal resistivity is influenced by collision with not only lattices, but also with impurity atoms and lattice defects. Additional scattering processes become significant only when the electron mean free path is of comparable magnitude to, or greater than, the separation between the scattering centres. The m.f.p. of conduction electrons in metals at room temperature is of the order of several tens of nanometers. Surfaces of continuous metal films of this thickness or less will cause additional scattering of the electrons. The film resistivity will be affected when such surface scattering is diffuse (i.e. electrons do not have any preferred direction after the interaction). If, on

the other hand, the scattering is specular, the magnitude of film resistivity remains unaffected. Two possible mechanisms determining the specular/diffuse scattering ratio are the presence of charge impurities on the surface and electron–phonon interaction at the surface, as proposed by Greene [12, 13].

2.1.3. Conduction in discontinuous metal films

The growth phenomena of thin films indicate that, in the early stages of growth, films are made up of small islands which may or may not be physically connected. At this stage, the study of electrical properties of metal films has exhibited "anomolous behaviour". The negative temperature coefficient of resistance, a.c. conduction, the non-ohmic behaviour, etc., have created sufficient interest in the mechanism of electron conduction in very thin films. The electrical conduction in these films is quite complex because more than one mechanism occurs simultaneously during such a transport process. The mechanism of charge transport in metallic films has been reviewed by Neugebauer and Wilson [14], Maissel [1] and Borziak and Kulyupin [8] among others. The various models proposed are briefly summarized as follows.

2.1.3.1. Thermionic emission. This model explains the conduction of electrons between two islands (separated by distance d) on the basis of thermionic emission [15–17]. Two islands, assumed to be charged, are considered equivalent to two separated electrodes, and the barrier maximum is assumed to exist half-way between the electrodes. Application of a small voltage reduces the barrier height. The conductivity, σ, is thus given as [1]

$$\sigma = \frac{BeT}{k_B} d \exp\left(\frac{\phi - Ce^2/d}{k_B T}\right) \qquad (3)$$

where B is a constant characteristic of the film geometry, ϕ the work function, e the electron charge, d the distance between the islands, C a constant, T the absolute temperature and k_B is the Boltzmann constant. This model is found to be applicable only to those structures having large island separation and low potential barriers. The predicted current densities are much smaller than those observed in practice.

2.1.3.2. Thermally activated tunnelling. The basic physics of conduction in discontinuous metal films in the regime of activated conductivity is generally believed to be that of the model by Neugebauer and Webb [18]. This model pictures a large number of islands, N, of which a relatively small number are charged. Tunnelling of charge between two islands is possible only if the energy level between them is crossed, i.e. their widths overlap. Normally since the barrier natures are quite different, an overlap is difficult. Hence, an activated electron renders a tunnelling of electrons more probable. Conductivity can be expressed as [18]

$$\sigma = C \exp -(2\mu^* d + E/k_B T) \qquad (4)$$

where μ^* is the tunnelling exponent for the wave function of electrons in the insulating region, d is the distance between grains and E is an effective activation energy. The tunnelling factor represents the dependence on island separation, of the mobility of the charge, in moving from grain to grain. This mechanism is applicable to a film consisting of small metal islands with small spacing between them. In such a situation, the activation energy is large and the tunnelling path length is short. The conductivity based on simple tunnelling predicts much lower conductivity than is observed experimentally.

2.1.3.3. Tunnelling between allowed states. Hartman [19] has suggested that quantum effects should be taken into account in small metallic islands with a linear dimension of 10 nm containing 10^4 atoms. In this situation, the electron energy levels will be quantized with an energy between levels of the order of 0.01 eV. The transport then consists of a thermal activation from the ground state to an excited state in one island, followed by tunnelling between excited states of different islands. The tunnelling between allowed near-neighbour states cannot explain the observed behaviour if there is no correlation between grain size and separation. In this model, the activation energy is calculated on the basis of separation of the lowest and next highest states of the potential well formed by the islands. The activation energies calculated based on this model are much smaller than those reported experimentally.

2.1.3.4. Substrate assisted tunnelling. Amorphous, insulating or conducting materials are normally used as substrates to deposit metallic films, and hence play an important role in the process of

electron conduction in films. The substrates have numerous traps between their conduction and valence bands and offer better routes for electron transfer than tunnelling through vacuum between islands [19, 20]. The transfer by the way of substrate is either through traps, hopping or by thermionic emission into the conduction band of the insulator that constitutes the substrate. Substrate-assisted tunnelling is most important for islands with relatively large spacing between them. The probability of such substrate-assisted tunnelling is even higher in metals, because the barrier height is less and the activation energy is smaller.

2.1.3.5. Variable-range hopping. This model was first proposed by Mott [21] in connection with amorphous materials. In this model, an electron chooses the distance it tunnels to optimize the balance between tunnelling and activation. Such models have not been explored because tunnelling beyond near-neighbour seems unlikely *a priori* in discontinuous metal films, in view of the considerably greater tunnelling distances involved in the process of conduction. However, the great intensity of the observed current has also been explained by the fact that free carriers created by both thermionic emission and tunnelling are injected into dielectric material of the substrate, where they are transferred from trap to trap by a hopping process.

Temperature dependence of conductivity in discontinuous films is influenced by many factors. In general, the temperature change induces a change in the conductivity of both individual islands and substrate. Owing to thermal expansion, a change is to be expected in the dimension and distances, which in turn may have great effect on the tunnelling probability. The thermionic energy supplied to the electrons is also changed. Furthermore, secondary changes may occur which can substantially modify the current. Although there are several models proposed in recent years to account for the temperature dependence of the conductivity in discontinuous systems [22–25], at present there are no satisfactory explanations for the observed temperature dependence of conductivity in metal films.

To understand clearly the conduction in discontinuous films, it is necessary to know the structure of these films during the early stages of formation. Recently, a statistical model has been proposed [26, 27] to describe the structure of discontinuous metal films in their coalescence stage of growth. This model is based on predictions from atomistic absorption and nucleation theories. Excellent agreement is achieved between this model and some of the experimental results on noble metal films.

2.1.4. Conduction in continuous metal films

At higher thicknesses the isolated islands in the film structure grow in size and coalesce to form a continuous film. The thickness at which a film becomes continuous is dependent on the type of material and various deposition parameters such as substrate temperature, deposition rate, vacuum and substrate.

There are several theoretical models proposed in recent years to account for the experimental results in continuous metal films. In what follows, we briefly summarize the important results of these theoretical models.

2.1.4.1. Thomson model. It was Thomson [28] who first postulated the concept of surface scattering when he was studying the variations of the conductivity of thin metal films. Thomson made the following important assumptions in his model:

(i) when an electron collides with the surface of the film (which are perfectly plane parallel), the probability of it being scattered in a solid angle $d\omega$ is $d\omega/2\pi$ and is independent of the initial and final direction of the electron motion,

(ii) the m.f.p. of an electron in the bulk metal, l_0, is a constant and it is greater than the film thickness, t, and

(iii) the conduction electrons behave as free electrons.

The expression for conductivity based on Thomson model is

$$\frac{\sigma_f}{\sigma_b} = \frac{t}{2l_0}\left(\log\frac{l_0}{t} + \frac{3}{2}\right) \tag{5}$$

where σ_f and σ_b are film and bulk conductivity, respectively. The Thomson model predicts that the conductivity of a thin film will be equal to 75% of that of the bulk material if the film thickness is just equal to the m.f.p., l_0. The serious objection to the model is that the film conductivity σ_f does not approach bulk conductivity σ_b in Equation 5 as $t/l_0 \rightarrow \infty$.

2.1.4.2. Fuchs model. In 1938, Fuchs [29] suggested that the assumptions made by Thomson were incorrect. Thomson had considered the free path of one electron and integrated to obtain the mean value. However, since all the electrons in the film are not identical to one another, all electrons must be considered to calculate the average value. Thomson had also neglected the free paths of the electrons at the surface, which have relatively very small values. Fuchs also pointed out the incorrect assumption of l_0 as constant. The statistical distribution of l_0 in the bulk is necessary to formulate a satisfactory model.

Thus, Fuchs developed a better relation for the conductivity of thin films, considering the random scattering from the film surfaces. The conduction electrons are assumed to be diffusely scattered at the surfaces and lose their momentum in the direction of the applied electric field, i.e. all the electrons are unspecularly reflected. An expression for conductivity is derived by considering the statistical distribution of all electrons and solving the Boltzmann transport equation with the appropriate boundary conditions. The result is expressed as the ratio of film to bulk conductivity in terms of film thickness and the electron m.f.p. as [30]

$$\frac{\sigma_f}{\sigma_b} = 1+\frac{3}{4}\left(\lambda-\frac{\lambda^3}{12}\right)B(\lambda)-\frac{3}{8\lambda}(1-e^{-\lambda}) - \left(\frac{5}{8}+\frac{\lambda}{16}-\frac{\lambda^2}{16}\right)e^{-\lambda} \quad (6)$$

where σ_f – film conductivity, σ_b – bulk conductivity, $\lambda = t/l_0$ and $B(\lambda) = \int_\lambda^\infty (e^\lambda/\lambda)d\lambda$. Equation 6 can be approximated for convenience as [3]

$$\frac{\sigma_f}{\sigma_b} = \left(1-\frac{3}{8\lambda}\right) \quad \text{for } \lambda \gg 1 \quad (7)$$

$$\frac{\sigma_f}{\sigma_b} = \frac{3}{4}\lambda\ln\left(\frac{1}{\lambda}\right) \quad \text{for } \lambda < 1 \quad (8)$$

2.1.4.3. Sondheimer approximation. The above model can suitably be modified when all the electrons are not diffusely scattered, but a fraction, p, gets specularly reflected from the surfaces. Thus, Equation 6 was slightly modified by introducing the directionality concept. The specularity parameter, p, defined as the ratio of electrons reflected at an angle, θ, to the normal, to the electron incident at an angle θ, is introduced, thus modifying the boundary conditions of the Boltzmann transport equation. Thus, the conductivity relation in the Sondheimer approximation [31] is

$$\frac{\sigma_f}{\sigma_b} = \left[1-\frac{3}{8\lambda}(1-p)\right] \quad \text{for } \lambda \gg 1 \quad (9)$$

$$\frac{\sigma_f}{\sigma_b} = \frac{3}{4}\lambda\frac{(1+p)}{(1-p)}\ln\left(\frac{1}{\lambda}\right) \quad \text{for } \lambda < 1 \quad (10)$$

These expressions (Equations 9 and 10) are known as Fuchs–Sondheimer equations and are extensively used to analyse experimental results. It is obvious from these equations that for electrons which undergo complete specular reflection ($p = 1$), the conductivity is not thickness dependent. Since the film surface is generally rough compared to the wavelength of conduction electrons, the scattering tends to be almost diffuse ($p = 0$). The size effect is caused by diffuse scattering of free charge carriers at the surface of thin films, therefore the specularity parameter is of fundamental importance. Determination of p from the experimental results is far from unique. Almost all the values of p lie between 0 and 1, and even unphysical values of $p < 0$ are used to explain experimental results. The magnitude of the surface scattering effect can be appreciated by referring to Fig. 1 in which computed curves of Campbell [32] are shown.

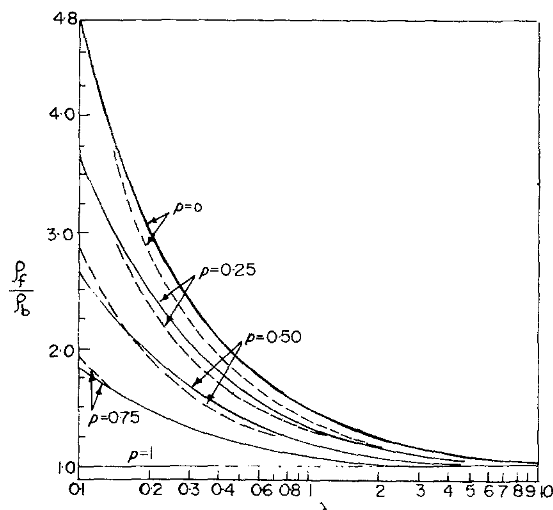

Figure 1 Theoretical size dependence of film conductivity. The solid curves are exact as calculated from Equation 6 while the dashed curves are calculated from the approximate Equation 9 (after [32]).

2.1.4.4. Useful approximations of Fuchs–Sondheimer model. Equations 9 and 10 hold good for very large and very small values of λ, respectively, but tend to be much in error for values of λ close to unity. It has been common practice to calculate the conduction electron m.f.p. using these equations and these values tend to be much greater than the values reported for bulk materials. Borrajo and Heras [33] have suggested the use of the following approximate equation:

$$\frac{\rho_f}{\rho_b} = 1 + 0.46/\lambda \qquad \text{for } \lambda \geqslant 0.5 \qquad (11)$$

in place of Equation 9. This equation gives satisfactory results for values of $\lambda > 0.5$. Recently Krishnamurthy and Shivakumar [34] have attempted to further refine the approximate Equation 9 for the case of diffuse scattering as follows:

$$\frac{\rho_f}{\rho_b} = 1 + \frac{Y}{\lambda} \qquad (12)$$

where Y is the ordinate intercept in the graph of $\lambda(\rho_f/\rho_b)$ against λ. It is suggested that the resistivity ratio with λ lying in the range 0.001 to 100 can be calculated using the above relation (Equation 12) with an accuracy of about 1%.

Although Fuchs–Sondheimer (FS) theory is widely used to analyse experimental results in metal films, it has numerous inherent shortcomings. Over the years, these expressions have been modified to render a better explanation of the thickness dependence of conductivity. The theory has the following deficiencies.

(i) A spherical Fermi surface is assumed. The fact that metals, especially in thin film form, have no simple structure means they have a distorted Fermi surface. It is not so easy to decide what are the most appropriate definitions of specular and diffuse scattering if the Fermi surface is not spherical.

(ii) FS theory considers only the geometric size effect and completely neglects the significant contribution from defects, imperfections, contaminations, chemical changes like oxidation and scattering at the crystallite boundaries.

(iii) FS theory assumes that there is no explicit dependence of the relaxation time τ on energy, while the recent calculations reveal [35–37] the explicit dependence of relaxation time on energy, depending on the scattering mechanism involved.

(iv) The FS relation for conductivity includes three transport parameters p, l_0 and σ_b. To determine these values simultaneously, they are assumed to remain constant. This is actually not true, since each film has its characteristic values of these parameters.

(v) It is assumed that the value of p is the same for upper and lower film surfaces. But it is actually different at the two interfaces.

(vi) It is experimentally established that the thickness against resistivity dependence in very thin films depends very much on the prevailing environment during deposition. There is no factor in Equations 9 and 10 that varies with deposition parameters (except p, partly).

(vii) FS theory assumes a film to be a single crystal, plane parallel slab. But in practice, a thin film structure is made up of an array of randomly oriented polycrystallites called "grains".

(viii) Fuchs took p as a constant, i.e. independent of the direction of incidence. FS theory also assumes that bulk m.f.p., l_0, is independent of thickness.

(ix) FS theory is strictly valid for monovalent metals and does not take into account the factors such as magnetic wall scattering and the presence of mixed phases. Hence, FS theory is not suitable to analyse experimental results of ferromagnetic metal films.

In the following discussion we briefly summarize the important models proposed in recent years, which try to overcome some of these above-mentioned drawbacks of the FS theory.

2.1.4.5. Lucas model. Since the interfaces on the two sides of the film surface are different (film and substrate, film and air), it is natural to expect a difference in the diffusivity of electrons from both the surfaces. Lucas [38] introduced different scattering coefficients (specularity parameters) p and q, for the upper and lower film surfaces. This makes FS Equations 9 and 10 more realistic as follows:

$$\frac{\sigma_f}{\sigma_b} = \left\{1 - \frac{3}{8\lambda}\left[1 - \frac{(p+q)}{2}\right]\right\} \qquad \text{for } \lambda \geqslant 1 \; (13)$$

$$\frac{\sigma_f}{\sigma_b} = \frac{3}{4}\frac{(1+p)(1+q)}{(1-pq)}\lambda \ln\left(\frac{1}{\lambda}\right) \qquad \text{for } \lambda < 1 \; (14)$$

2.1.4.6. Parrott–Cotti model. Parrott [39] has objected to the assumption of a constant

specularity parameter and has suggested that p should depend on the electron wavelength and angle of incidence. Brändli and Cotti [40] have improved the FS model by introducing an angular dependence of p on the critical angle of incidence, θ_c, with respect to the film normal:

$$p(\theta) = 0 \quad \text{when } 0 < \theta < \theta_c$$
$$= 1 \quad \text{when } \theta_c < \theta < \pi/2 \qquad (15)$$

When the critical angle $\theta_c = \pi/2$, the resistivity has the same thickness dependence as that obtained by Fuchs for $p = 0$. For any critical angle $\theta_c < \pi/2$, the resistivity, contrary to the results of Fuchs, approaches a constant finite value, as the film thickness, t, decreases to zero. Thus, Brändli and Cotti have considered only two extreme cases of the FS model. So the experimental results could not agree with this model, even to the extent of the FS model.

Ziman [11] solved the transport equation by considering an ellipsodal Fermi surface and concluded that the film conductivity and electron mobility decreases to a limiting value, rather than decrease infinitely as predicted by FS theory. Engleman and Sondheimer [41] have considered a general non-spherical Fermi surface and have shown that the conductivity also exhibits anisotropic behaviour. Ziman [11] also tried to modify the boundary conditions employed by Fuchs, and included a collision operator to define the incidence and collision of electrons, along with specularity parameter p. But because of the lack of detailed knowledge of the surface structure, reflection could only be characterized by the statistical parameters.

2.1.4.7. Soffer model. Soffer [42] has extended Ziman's discussion of the scattering problem at the surface. Ziman had not taken into account the necessity of conserving the net flow of electrons corresponding to the incident and the reflected waves. When the same assumptions are made, about the correlation function of the height of the surface asperities as in the Ziman theory, the specularity parameter, p, exhibits an angular dependence given by the following equation:

$$p(\cos\theta) = \exp\left(-\frac{16\pi^2 h^2}{k_0^2}\cos^2\theta\right) \qquad (16)$$

$$\frac{\sigma_f}{\sigma_b} = \frac{3}{4}\lambda\left(\frac{2+G}{G}\right)\ln\left(\frac{1}{\lambda}\right) \qquad \text{for } \lambda \ll 1 \ (17)$$

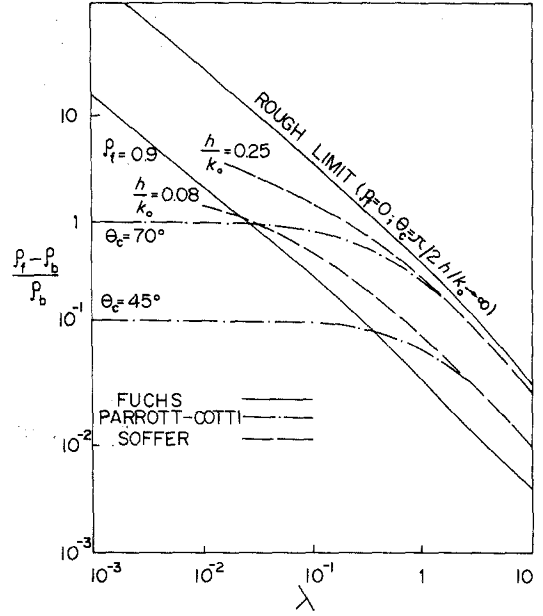

Figure 2 The size effect in electrical resistivity according to the FS model, Parrott–Cotti model and Soffer model (after [30]).

where $G = (16\pi^2 h^2/k_0^2)$, h is the r.m.s. of the height of surface roughness, k_0 is the electron wavelength and θ is the angle of incidence of conduction electrons measured from the surface normal. In this model p approaches a constant finite value when the film thickness approaches zero. Soffer results for the thickness dependent resistivity lie between those of Parrott–Cotti and FS models for $p = 0$ (Fig. 2).

Recently, Grendel [43] has refined the definition of the specularity parameter, p, by taking into account the degeneracy of the conduction electron gas. He has suggested the use of the effective specularity parameter, p_g, in the Fuchs-type boundary conditions to solve the Boltzmann equation:

$$p_g = p\frac{1-f_0}{1-p^2 f_0} \quad \text{for a degenerated gas}$$
$$= p \quad \text{for a non-degenerate gas} \qquad (18)$$

where f_0 is the Fermi–Dirac distribution function. For most metals $p \approx 0$, so it is immaterial to distinguish between p and p_g.

2.1.4.8. Ghodgaonkar, Tillu and Ramani model. Recently, Ghodgaonkar and co-workers [44, 45] have examined the possible dependence of the

specularity parameter, p, on the critical angle by discarding the possibility of assigning a constant value to it. The angular dependence of the specularity parameter is given by [44]

$$p(\theta) = \exp(-\pi/2)(\cos\theta_c/\cos\theta) \quad (19)$$

and the thin film conductivity is given by [44]

$$\frac{\sigma_f}{\sigma_b} = \frac{4\pi\cos\theta_c + 2\lambda}{\lambda\left[8 + 3\pi\cos\theta_c \ln\left(\frac{1}{\lambda}\right)\right]} \quad (20)$$

Fig. 3 shows the comparison of experimental results with different models. Although Equation 20 proposed by Ghodgaonkar and co-workers gives a better fit to the experimental results compared to other models, the agreement is far from satisfactory.

Despite all the physical arguments, the possible dependence of p is a matter of speculation for a given size dependent thin film experiments. The main difficulty arises due to its artificial introduction in the FS theory. Ghodgaonkar and Ramani [45] have introduced a general interaction parameter, θ^*, in the FS distribution function, which takes values from 0 to 1 and is coupled to the velocity term and hence reflects a wavelength dependence. In this formalism thin film conductivity is expressed as

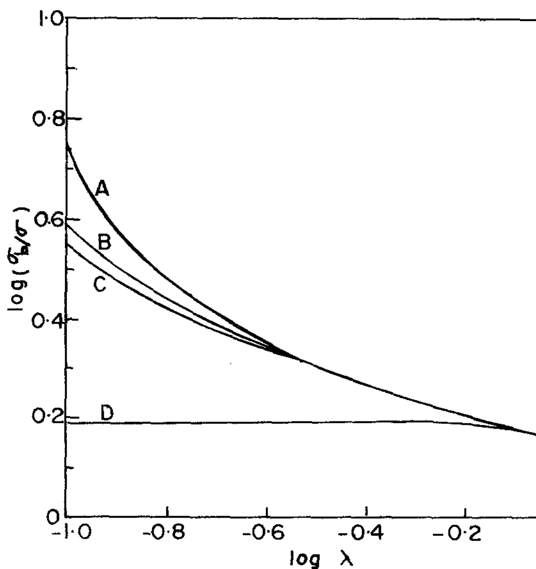

Figure 3 Comparison of experimental results A, Worden–Danielson (*J. phys. Chem. Solids* 6 (1958) 89) with three theoretical models; B, Ghodgaonkar–Tillu; C, Fuchs–Sondheimer; D, Brändli–Cotti $p = 0.5$, $\theta_c = 78.4°$ (after [44]).

$$\frac{\sigma_f}{\sigma_b} = \frac{3\lambda}{4\theta^*}\ln\left(\frac{1}{\lambda}\right) \qquad \text{for } \lambda \ll 1 \quad (21)$$

where θ^* is the memory indicator. On comparing Equation 21 with Equations 9 and 10,

$$\theta^* = (1-p) \qquad \text{for } \lambda \gg 1$$
$$\theta^* = \frac{(1-p)}{(1+p)} \qquad \text{for } \lambda \ll 1 \quad (22)$$

Thus, this improved model leads to different values in thick and thin film limits for the relation between the memory indicator, θ^*, and the specularity parameter, p, thereby indicating that the two formalisms are not identical. This model seems to provide a better fit with the experimental data. Although the memory indicator, θ^*, serves as a good adjustable parameter to fit the experimental data, no physical interpretation of the term has been given by these authors [45].

The disagreement between experiment and theory is quite appreciable when the sample thickness falls below about 50 nm. In general, the resistivity of such thin films is well above that which can be predicted by any theory utilizing the linear Boltzmann equation. It is apparent from the structural studies of thin films that, in addition to microscopic roughness, there exists a macroscopic roughness due to the granularity of the films. Often films are observed to have a complex channelled structure with metal grains connected via percolation paths. For even thinner films the islands become disconnected, the films cease to conduct in an ohmic manner, and effects of inter-island hopping are observed. Wedler *et al.* [46] have suggested that there exists a critical thickness below which the films of a particular metal have sufficient channels to prevent normal conduction and that, above this value, there is an effective sample thickness which is the mean thickness less the critical value.

2.1.4.9. Namba model. Namba [47] has proposed the inclusion of the geometrical heterogeneous film cross section due to surface roughness into the expression for resistivity, by considering a conductor whose thickness, t, varied sinusoidally as a function of a one-dimensional position co-ordinate, x, along its length, L. The approximation used was thus

$$t(x) = t_0 + h\sin 2\pi x/L \quad (23)$$

where t_0 is the mean film thickness, h is a measure of the macroscopic roughness, x is the period of the surface structure and L is the length of the film. FS theory was then used, assuming a value of the bulk m.f.p., l_0, to obtain $\rho_f(t)/\rho_b$. Thus the overall film resistivity, ρ_f, is expressed as

$$\frac{\rho_f}{\rho_b} = \frac{t_0}{L}\int_0^L \frac{\rho[t(x)]}{t(x)}\,dx \qquad (24)$$

where $\rho[t(x)]$ is the resistivity according to FS theory. The integral of Equation 24 cannot be traced analytically. All experimental results can be fitted by Equation 24 using h as the fitting parameter. The Namba model leads to a stronger decrease in the conductivity with decreasing film thickness than all other models discussed so far. Ohmic conductivity is zero as long as the mean film thickness is smaller than the surface roughness. There are three main weaknesses of this model: (i) the actual sample thickness is poorly approximated by a sine function, (ii) the model is essentially one-dimensional, no percolation effects are possible and (iii) the model is not applicable to ultra-thin films in which conduction is by tunnelling.

2.1.4.10. Elsom and Sambles model. Elsom and Sambles [48] have recently tried to overcome some of the limitations of the Namba model by using more realistic sample conditions. These authors have used a new method for the modelling of the conduction properties of semi-islandized films, and have shown how the effects of macroscopic roughness lead to the enhancement of resistivity. It is shown that the effect of island growth changes resistivity in a different manner to that of changing the m.f.p., l_0. Consequently, the resulting theoretical ρ_f/ρ_b against λ curves for varying l_0 are quite different to those for varying t_0. Although this model seems to be in agreement with many experimental results on transition metal films, the predictions are valid only at high temperatures and for $\lambda > 0.15$.

2.1.4.11. Cottey model. An alternative expression for the FS function has been proposed by Cottey [49] who considered only continuous metal films with smooth parallel surfaces. Cottey assumed that: (i) the free electron model is valid, (ii) bulk and surface scattering are taking place independently, (iii) the bulk m.f.p. of conduction electrons is independent of position, film thickness and direction of motion of electrons and (iv) the FS model is valid with $(1-p) \ll 1$. The function describing size effect in the conductivity $F(\eta)$ is written in the form [49]

$$F(\eta) = \frac{\sigma_f}{\sigma_b} = \frac{3}{2}\eta\left[\eta - \frac{1}{2} + (1-\eta)^2 \ln\left(1 + \frac{1}{\eta}\right)\right] \qquad (25)$$

$$\frac{\sigma_f}{\sigma_b} = \left(1 - \frac{3}{8\eta} + \frac{1}{5\eta^2} - \frac{1}{8\eta^3} + \frac{3}{35\eta^4} - \ldots\right) \quad \text{for } \eta > 1 \qquad (26)$$

$$\frac{\sigma_f}{\sigma_b} = \left(\frac{3}{2}\eta \ln\frac{1}{\eta} - \frac{3}{4}\eta + 3\eta^2 - \frac{3}{2}\eta^2 \ln\frac{1}{\eta} - \ldots\right) \quad \text{for } \eta < 1 \qquad (27)$$

where $\eta = \lambda(1-p)^{-1}$. The Cottey model is reliable as the exact solution of the FS model for most actual cases with $p \geq 0.8$. It is pointed out [50] that this model is a more general tool for studying transport properties and may facilitate the numerical evaluations of most of the transport properties.

2.1.4.12. Mayadas–Shatzkes model. Because the typical grain size is often comparable to the electron m.f.p., the contribution of crystalline boundaries to electron scattering increases with decreasing film thickness. It is expected that scattering at the grain boundaries will make a significant contribution to the film resistivity. Consequently, as long as the crystalline size is smaller than the electron m.f.p. the FS model cannot be applicable. The grain boundaries are of arbitary shapes, sizes and orientation and the scattering due to them occurs simultaneously with an isotropic background (scattering due to defects, impurities and phonons, etc.). Thus, computation of the electron velocity distribution, for scattering from grain boundaries, presents enormous difficulties. To simplify the problem, Mayadas–Shatzkes (MS) [51] made the following assumptions.

(i) The grains are not symmetric three dimensionally. They tend to grow in a columnar fashion

and the average grain diameter is equal to the thickness of the films.

(ii) Only grain boundaries whose normals lie in the film plane contribute to the scattering. The grain boundaries can be represented by randomly spaced planes that are either parallel or perpendicular to the electric field **E**. Other orientations of the grain boundaries are assumed to be negligible.

(iii) It was assumed that the grain boundaries could be represented by a δ-function, so that all the parallel boundaries lead to specular reflection [52].

(iv) The computation includes determination of the grain boundary resistivity ρ_g caused by electron scattering from a series of partially reflecting randomly spaced planar grain boundaries, which occur simultaneously with the isotropic background. This required that an estimate be made of the relaxation time for grain boundary scattering. Mayadas–Shatzkes obtained a new relaxation time, τ_g, in terms of a structural parameter, α, which described the geometry of a grain and the scattering power of its boundaries:

$$\alpha = \frac{l_0}{D}\frac{R}{(1-R)} \tag{28}$$

where D is the average grain diameter, R is the grain boundary reflection parameter with values between 0 and 1. R is found to be dependent on (i) the grain boundary type, (ii) impurities absorbed at grain boundaries, and (iii) the intergrain geometry and radius of curvature. The MS model can be summarized by the following equation [53]:

$$\sigma_f = \sigma_b\,[f(\alpha) - A] \tag{29}$$

where

$$A = \frac{6}{\pi\lambda}(1-p)\int_0^{\pi/2} d\phi \int_1^{\infty} \frac{\cos^2\phi}{H^2(u,\phi)}\left(\frac{1}{u^3}-\frac{1}{u^5}\right) \times \frac{1-\exp[-\lambda u H(u,\phi)]}{1-p\exp[-\lambda u H(u,\phi)]}\,du \tag{30}$$

$$f(\alpha) = 1 - \frac{3}{2}\alpha + 3\alpha^2 - 3\alpha^3\left(1+\frac{1}{\alpha}\right) \tag{31}$$

$$H(u,\phi) = 1 + \alpha(\cos\phi)^{-1}\left(1-\frac{1}{u^2}\right)^{-1/2} \tag{32}$$

The ratio of the film to bulk resistivity, inclusive of grain boundary scattering effect, can be simplified as follows [53]:

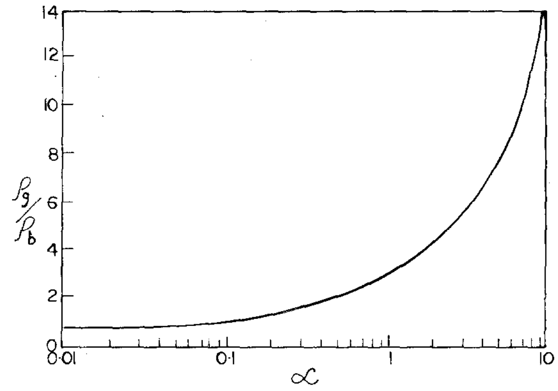

Figure 4 The effect of grain-boundary scattering on a bulk material (after [51]).

$$\frac{\rho_b}{\rho_g} = 3\left[\frac{1}{3} - \frac{1}{2}\alpha + \alpha^2 - \alpha^3 \ln\left(1+\frac{1}{\alpha}\right)\right] \tag{33}$$

$$\frac{\rho_b}{\rho_g} = 1 + \frac{3}{\alpha} \quad \text{for } \alpha \gg 1; \qquad \frac{\rho_b}{\rho_g} = \frac{3}{4\alpha} \quad \text{for } \alpha \ll 1 \tag{34}$$

where ρ_g is the infinitely thick polycrystalline film resistivity. This function is shown in Fig. 4 where it is seen that for small values of α, $\rho_g \to \rho_b$.

2.1.4.13. Tellier, Pichard and Tosser approximation. Tellier and co-workers [54–56] have used the concept of an effective relaxation time τ_g to describe the simultaneous process of background and grain boundaries in polycrystalline and monocrystalline films. The relaxation time, τ_g, and effective m.f.p., l_g, in polycrystalline films are related to the grain-boundary function $f(\alpha)$ by the following expression [56]:

$$\tau_g = \tau_b f(\alpha) \qquad l_g = l_0 f(\alpha) \tag{35}$$

and the effective reduced thickness is given by

$$\lambda_g = t/l_g \tag{36}$$

In the limit of very thin polycrystalline films the general expression of the film resistivity becomes [54]

$$\frac{\rho_f}{\rho_g} = \frac{4(1-p)}{3(1+p)}\frac{1}{\lambda_g}\frac{1}{\ln\left(\frac{1}{\lambda_g}\right)+0.4228} \quad \text{for } \lambda_g < 1 \tag{37}$$

$$\frac{\rho_f}{\rho_g} = 1 + \frac{3}{2}\alpha + \frac{3}{8\lambda_g}(1-p) \quad \text{for } \lambda_g > 1 \qquad (38)$$

In case of $\alpha = 0$, the MS Equations 37 and 38 reduce to the FS Equations 9 and 10. The grain size increases with increasing film thickness upto a certain limit. Thereafter, the number of the grains start increasing due to fresh nucleation centres so that the grain size does not increase any further. Thus, the use of MS relations is valid for low thickness films, after which pure size effect prevails.

2.1.4.14. Mola and Heras approximation. Mola and Heras [53] have calculated film resistivity for a wide range of λ and these do indeed demonstrate that for small grain sizes the dominant contribution to the additional resistivity arises from boundary rather than surface scattering. For the study of size effect in thin films, thickness ranging from 10 to 100 nm are usually used and the experimental electron m.f.p. values are in the range 10 to 50 nm. Hence, λ takes values ($0.2 \leqslant \lambda \leqslant 5$) close to unity and in this range it is incorrect to use an approximate equation for thick films ($\lambda \gg 1$) or thin films ($\lambda \ll 1$). Mola and Heras [53] have linearized the exact equations of the MS model and have given the following approximate equation:

$$\frac{\rho_f}{\rho_b} = 1 + \frac{3}{8\lambda}\left(\frac{3R+1}{1-R}\right)(1-p) \qquad (39)$$

2.1.4.15. Wedler and Wissmann approximation. Wissmann [57] and Wedler and Wissmann [58] obtained a useful approximation of the MS model as

$$\frac{\rho_f}{\rho_b} = 1 + m\frac{l_0}{D} + \frac{3}{8\lambda}(1-p) \qquad (40)$$

where m is a phenomenological factor having no concrete physical meaning and this term describes the grain boundary contribution to resistivity. This relation provides a useful framework to interpret resistivity data. This approximation is, however, valid [59] for not too thick films and the grain boundary influence on the electrical resistivity is not too strong. Recently, Tellier *et al.* [60] have suggested a physical expression to this phenomenological term "m";

$$m = 1.144 \ln\left(\frac{1}{\nu}\right) \qquad (41)$$

where ν is the transmission coefficient through grain boundaries.

2.1.4.16. Falkovsky approximation. Taking surface correction into account Falkovsky [61] has modified Equation 39 for electrical resistivity as follows:

$$\frac{\rho_f}{\rho_b} = \frac{3}{8\lambda}\frac{(3R+1)}{(1-R)}(1-p) + \left\{3\lambda\left[\frac{1+2\lambda}{(2\lambda^{1/2})}\right] \text{arctgt}\left[\left(\frac{1}{2\lambda}\right)^{1/2} - 1\right]\right\} \qquad (42)$$

Many authors have used this modified MS equation and find it a better fit with the experimental data.

2.1.4.17. Ghodgaonkar and Ramani approximation. Ghodgaonkar and Ramani [62] have extended the scope of the MS model by incorporating the Lucas model for thin films with unlike surfaces characterized by specularity parameters, p and q, and to set up a distribution function which will eventually lead to the calculation of the film conductivity. The ratio of film and bulk conductivity is expressed as

$$\frac{\sigma_f}{\sigma_b} = [f(\alpha) - A'] \qquad (43)$$

where

$$A' = \frac{3}{\pi\lambda}\left\{\int_0^{\pi/2} d\phi \int_0^1 \frac{\cos^2\phi}{H^2(u,\phi)} du\,(u-u^3) \times \left[\frac{1-\exp(-\lambda H/u)}{1-pq\exp(-2\lambda H/u)}\right] \times [2-p-q+(p+q-2pq)\exp(-\lambda H/u)]\right\} \qquad (44)$$

Ghodgaonkar and Ramani assume specularity parameters p and q to be of constant value, and an unambiguous determination of these from experimental data is not easy. In generalizing the MS model, these authors have assumed that the product of thin film resistivity and m.f.p. is not constant, which was not taken into consideration in earlier models.

2.2. Temperature coefficient of resistance

2.2.1. Introduction

The temperature coefficient of resistance (TCR) is defined for bulk materials, β_b, and for films, β_f, by

$$\beta_b = \frac{1}{\rho_b}\frac{d\rho_b}{dT} \qquad \beta_f = \frac{1}{\rho_f}\frac{d\rho_f}{dT} \tag{45}$$

The temperature dependent component of resistivity originates from the interaction of electrons with phonons, whereas their scattering from lattice defects is practically temperature independent. The resistivity connected with the scattering on a surface is a function of λ. Only for rather thick film is the surface scattering independent of temperature, and we may write

$$\frac{d\rho_f}{dT} = \frac{d\rho_{ph}}{dT} = \frac{d\rho_b}{dT} \tag{46}$$

By using Equation 46 we write [63]

$$\beta_f\rho_f = \beta_g\rho_g = \beta_b\rho_b \tag{47}$$

where β_g is the infinitely thick polycrystalline film TCR.

2.2.2. Fuchs–Sondheimer approximation

From Equation 6 we can write

$$\frac{\rho_b}{\rho_f} = f(\lambda) = \frac{\beta_f}{\beta_b} \tag{48}$$

$$\frac{\partial\rho_f}{\partial T} = \frac{f(\lambda)\dfrac{\partial\rho_b}{\partial T} - \rho_b\dfrac{\partial f(\lambda)}{\partial T}}{[f(\lambda)]^2} \tag{49}$$

Using Equations 45 to 47, we write

$$\frac{\beta_f}{\beta_b} = \frac{f(\lambda) - \lambda\partial f(\lambda)/\partial\lambda}{f(\lambda)} \tag{50}$$

From the FS model the ratio of film to bulk TCR is expressed as

$$\frac{\beta_f}{\beta_b} = \left[1 - \frac{3}{8\lambda}(1-p)\right] \quad \text{for } \lambda > 1 \tag{51}$$

2.2.3. Mayadas–Shatzkes approximation

From the MS model the ratio of film to bulk TCR is expressed as [63],

$$\frac{\beta_f}{\beta_b} = \left[1 - \frac{3}{2}\alpha - \frac{3}{8\lambda}(1-p)\right] \quad \text{for } \lambda > 1 \tag{52}$$

Equations 51 and 52 can be used to determine values of β_b, l_0, p and R from the TCR data of only two films. It is expected that the TCR of a metal film will be considerably less than the pure bulk value since both surface scattering and impurity effects tend to reduce its value.

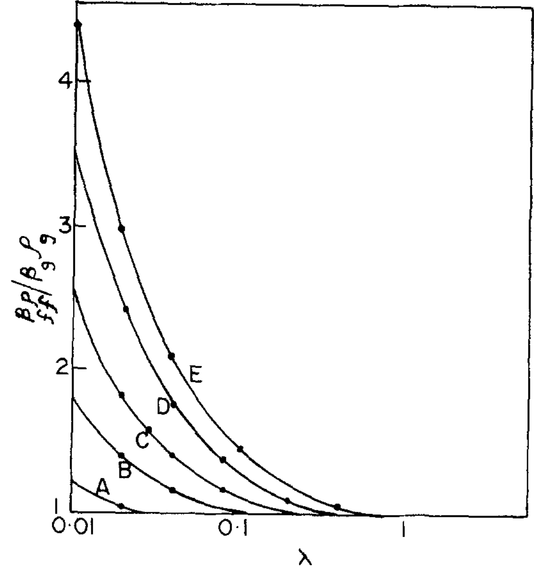

Figure 5 The thickness variation of the reduced product $\beta_f\rho_f/\beta_g\rho_g$ against λ for totally diffuse scattering ($p = 0$) for different values of α: A, 10; B, 5; C, 1; D, 0.75; E, 0.5 (after [54]).

2.2.4. Tellier, Pichard and Tosser approximation

Tellier *et al.* [54] have derived a very useful approximate expression for TCR in very thin polycrystalline films, in the light of the effective FS model as

$$\frac{\beta_f\rho_f}{\beta_g\rho_g} \approx \frac{4}{3}\left[\frac{(1-p)}{(1+p)}\left(\frac{1}{\lambda_g}\right)\right]\left[\ln\left(\frac{1}{\lambda_g}\right) + 0.4228\right]^{-2} \quad \text{for } \lambda_g < 1 \tag{53}$$

Equation 53 gives an analytical expression for variations in the ratio $\beta_f\rho_f/\beta_g\rho_g$ when the thickness values satisfy the above expression. Fig. 5 shows the thickness variations of the reduced product $\beta_f\rho_f/\beta_g\rho_g$ against λ.

2.2.5. Negative TCR

One of the most interesting phenomena exhibited by thin metallic films is the occurrence of negative TCR, although Matthiessen's rule predicts that the TCR should always be positive. The TCR has been observed to be negative for very low thickness and structurally discontinuous films. Generally, the greater the deviations of film resistivity from theoretical expectations, the greater will be the tendency of the TCR to be negative [1]. Trapped impurities and inherent film defects contribute to the negativity of the TCR. When the film

thickness is increased, due to gettering action, the impurities are less in the upper layer. The lower layer that has a host of impurities exhibits a strong negative TCR while that of the upper layer is strongly positive. Negative TCR is obtained also when the thermal coefficient of expansion changes with film material. This leads to further separation of the crystallites to render them more discontinuous. Trapped oxygen migrates into the film via the grain boundaries. Consequent oxidation, and hence insulation of the grain boundaries and small islands, tend to make the TCR of such films negative. The negative TCR can be expected to occur owing to some activated process and can be explained on the basis of thermionic emission or even tunnelling between islands. Neugebauer and Webb [18] have made a classification of evaporated films depending on their TCR: (i) when the film is around 100 nm, its TCR is positive and approaches bulk value, (ii) when the film thickness is about 10 nm, its TCR decreases with thickness and finally approaches zero and (iii) when the film thickness is about a few nanometers, it is characterized by negative TCR.

Vamadatt [64] has explained the occurrence of negative TCR in the case of ultra-thin films on the basis of the FS model. Differentiating Equation 10 with respect to temperature, we obtain the following expression for TCR of film [65]:

$$\beta_f = \beta_b + \chi \frac{\ln\left(\frac{1}{\lambda}\right) - 1}{\ln\left(\frac{1}{\lambda}\right)} \tag{54}$$

where $\chi = (1/l_0)(\mathrm{d}l_0/\mathrm{d}T)$ is the temperature coefficient of m.f.p. Since χ is, in general, negative, the film TCR can be expected to have a negative values for $\lambda < 0.368$.

In view of this, it is important to include terms which can account for expansion of the film thickness and film–substrate expansion mismatch in the expression for the TCR. The effect of thermal strains due to the difference in the thermal expansion coefficients on the TCR of film has been studied by several authors [65–69].

2.2.6. Verma and Sharma approximation

Verma and Sharma [66] have derived the following equation for the TCR taking into consideration the thermal expansion of the bulk material:

$$\beta_f = \beta_b - a_b + (\theta_1 + 1)\frac{\mathrm{d}\epsilon_1}{\mathrm{d}T} + (\theta_2 - 1)\frac{\mathrm{d}\epsilon_2}{\mathrm{d}T} + (\theta_3 - 1)\frac{\mathrm{d}\epsilon_3}{\mathrm{d}T} \tag{55}$$

where a_b is the thermal expansion coefficient of the bulk material, θ_1 is the longitudinal strain coefficient of resistivity in the bulk, θ_2, θ_3 are the transverse strain coefficients of resistivity, ϵ_1 and ϵ_2 are the strain in the plane of the film and ϵ_3 is the strain in the perpendicular direction. Equation 55 does not take size effect into account and hence is not suitable to analyse TCR results in thin films.

2.2.7. Warkusz model

Warkusz [68] has derived a general expression for the TCR of thin metal films taking into consideration (i) the influence of the external size effect on the film resistivity, (ii) thermal strain and (iii) the difference in the thermal expansion coefficient between the film and its substrate. An expression for the TCR of metal films without any substrate is given by [68]

$$\beta_f = \beta_b - (\beta_b + a_f)F(\lambda) \tag{56}$$

where, $F(\lambda) = [\lambda/f(\lambda)]\,[\partial f(\lambda)/\partial\lambda]$ and a_f is the thermal expansion coefficient of film. Fig. 6 shows a graph of β_f against λ for $p = 0$ and for $p = 0.5$ for some of the transition metal films.

Owing to mismatch in the thermal expansion coefficient between the film and its substrate, the film is subjected to stresses when the temperature is varied, and this leads to the appearance of thermal strain in the film which affects its resistivity. A general expression for the TCR of film attached to the substrate is given by [68]

$$\begin{aligned}\beta_f = {} & \beta_b - (\beta_b - a_b)F(\lambda) \\ & + [\theta_1 + 1 - F(\lambda)(n - w)]\frac{\mathrm{d}\epsilon}{\mathrm{d}T} \\ & + [\theta_2 - 1 - F(\lambda)(n - w)]\frac{\mathrm{d}\epsilon_2}{\mathrm{d}T} \\ & + [\theta_3 - 1 - F(\lambda)(n + 1)]\frac{\mathrm{d}\epsilon_3}{\mathrm{d}T}\end{aligned} \tag{57}$$

where a_b is the thermal expansion coefficient of bulk material, $n = -(1/l_0)(\mathrm{d}l_0/\mathrm{d}\epsilon_1)$ and $w = -(1/t)(\mathrm{d}t/\mathrm{d}\epsilon_2)$ are Poisson's ratios. If size effect is neglected, the above Equation 57 reduces to

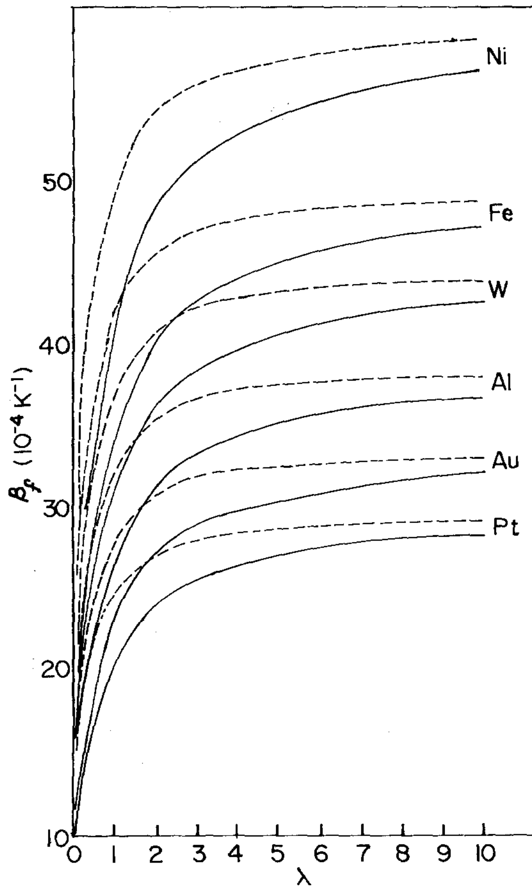

Figure 6 β_f against λ curves with (———) $p = 0$ and (– – – –) $p = 0.5$ for some transition metal films (after [68]).

Equation 55. Recent experimental results on chromium films [69] demonstrate the influence of thermal expansion of the substrate on the TCR of these films.

2.2.8. Mola and Heras model

Mola and Heras [53] have derived an exact expression for the dependence of the TCR on film thickness starting from the MS model. They have assumed that (i) the rigid band model for a metal is valid, (ii) the number of conduction electrons per unit volume is temperature independent and (iii) the thermal expansion of film, a_f, and of grain size, a_g, are negligible.

(i) Assuming that crystalline diameter, D, equals film thickness, the TCR of monocrystalline films is expressed as

$$\frac{\beta_f}{\beta_0} = 1 + \frac{g(\alpha) - A + B + C}{f(\alpha) - A} \tag{58}$$

where β_0 is the TCR of an infinitely thick monocrystalline film.

(ii) Assuming $\alpha \geqslant 0$ and is thickness independent, the TCR is expressed as

$$\frac{\beta_f}{\beta_0} = 1 + \frac{D - A}{f(\alpha) - A} \tag{59}$$

where

$$g(\alpha) = -\frac{3}{2}\alpha + 6\alpha^2 + \frac{3\alpha^3}{1+\alpha} - 9\alpha^3 \ln\left(1 + \frac{1}{\alpha}\right) \tag{60}$$

$$B = \frac{6}{\pi}(1-p)^2 \int_0^{\pi/2} d\phi \int_1^{\infty} \frac{\cos^2\phi}{H^2(u,\phi)} \left(\frac{1}{u^2} - \frac{1}{u^4}\right) \frac{\exp[-\lambda u H(u,\phi)]}{\{1 - p\exp[-\lambda u H(u,\phi)]\}^2} du \tag{61}$$

$$C = \frac{12\alpha}{\pi\lambda}(1-p) \int_0^{\pi/2} d\phi \int_1^{\infty} \frac{\cos\phi}{H^3(u,\phi)} \left(\frac{1}{u^2} - \frac{1}{u^4}\right) \frac{1}{(u^2-1)^{1/2}} \frac{1 - \exp[-\lambda u H(u,\phi)]}{1 - p\exp[-\lambda u H(u,\phi)]} du \tag{62}$$

$$D = \frac{6}{\pi}(1-p)^2 \int_0^{\pi/2} d\phi \int_1^{\infty} \frac{\cos^2\phi}{H(u,\phi)} \left(\frac{1}{u^2} - \frac{1}{u^4}\right) \frac{\exp[-\lambda u H(u,\phi)]}{\{1 - p\exp[-\lambda u H(u,\phi)]\}^2} du \tag{63}$$

Mola and Heras have evaluated analytically Equations 58 and 59 for different values of p. They have also suggested the use of the following approximate equations in place of Equations 58 and 59 to analyse experimental results:

$$\frac{\beta_f}{\beta_0} = \left[1 + \frac{1}{\lambda}P(p,R)\right]^{-1} \quad \text{for } t = D \tag{64}$$

$$\frac{\beta_f}{\beta_0} = \left[1 + \frac{1}{\lambda}Q(p,\alpha)\right]^{-1} \quad \text{for } \alpha \geqslant 0 \tag{65}$$

2.2.9. Pichard, Tosser and Tellier approximation

Tellier and Tosser [55] have given a more convenient form of Equation 58 for polycrystalline films. The TCR, β_g, of an infinitely thick polycrystalline film is given by

$$\frac{\beta_g}{\beta_0} = 1 + \frac{g(\alpha)}{f(\alpha)} \quad (66)$$

The experimental size effect in the polycrystalline film TCR is given by [55]

$$\frac{\beta_f}{\beta_g} = \left[1 + \frac{g(\alpha) - A + B + C}{f(\alpha) - A}\right]\left[1 + \frac{g(\alpha)}{f(\alpha)}\right]^{-1} \quad (67)$$

Pichard *et al.* [63] have also given an improved analytical expression for the TCR of film, starting from the MS model, taking into consideration the effect of thermal strain caused by the thermal expansion of film and the grains:

$$\frac{\beta_f}{\beta_b} = 1 + \frac{g(\alpha) - A + B + C}{f(\alpha) - A} + \frac{(D - A)a_f}{[f(\alpha) - A]\beta_0} + \frac{[g(\alpha) + B + C - D]}{f(\alpha) - A}\frac{a_g}{\beta_b} \quad (68)$$

$$\frac{\beta_f}{\beta_b} = 1 + X^* + Y^* a_f/\beta_b + (X^* - Y^*)a_g/\beta_b \quad (69)$$

where

$$X^* = [g(\alpha) - A + B + C]\,[f(\alpha) - A]^{-1} \quad (70)$$

$$Y^* = (D - A)\,[f(\alpha) - A]^{-1} \quad (71)$$

Pichard *et al.* [63] have also considered the effect of thermal expansion of the substrate on the TCR and have given the following general expression for the TCR of polycrystalline supported films:

$$\frac{\beta_f}{\beta_b} = 1 + X^* + Y^* a_f/\beta_b + (X^* - Y^*)a_g/\beta_b + [2(\theta + 1) + X^*(2\theta - n_f + 1) - Y^*(n_f + 1)](a_s - a_f)(1 - n_f)^{-1}\beta_b^{-1} \quad (72)$$

where n_f is Poisson's ratio of the film and θ is the strain coefficient of the bulk m.f.p.

2.2.10. *Jain and Srivastava approximation*

Jain and Srivastava [70] have recently derived an expression for TCR of supported films from the effective Cottey model:

$$\frac{\beta_f}{\beta_b} = \left[1 + \frac{g(\alpha)}{f(\alpha)}\right]\left\{1 - \frac{G(\eta_g)}{F(\eta_g)}[1 + a_f/\beta_b]\right\} + \frac{a_f}{\beta_b}\left\{\frac{g(\alpha)}{f(\alpha)} - \frac{G(\eta_g)}{F(\eta_g)} \times \left[\frac{2n_f(1 - a_s/a_f)}{(1 - n_f)}\right]\right\} \quad (73)$$

where

$$F(\eta_g) = \frac{3}{2}\eta\left[\eta - \frac{1}{2} + (1 - \eta)^2 \ln\left(1 + \frac{1}{\eta}\right)\right] \quad (74)$$

$$G(\eta_g) = \eta_g \frac{\mathrm{d}F(\eta_g)}{\mathrm{d}\eta_g} \quad (75)$$

and

$$\eta_g = \frac{\lambda}{f(\alpha)}(1 - p)^{-1} \quad (76)$$

If the film–substrate expansion mismatch and the expansion of the average grain diameter is neglected, i.e. $a_s = a_f = 0$, Equation 73 reduces to the approximation expression (Equation 9) of Tellier and Tosser [71].

2.3. Thermoelectric power (TEP)

The transport equation suggests that the perturbation of electron distribution is also caused by a thermal gradient. A potential difference is created across a sample which is subjected to a thermal gradient. The thermal e.m.f. generated per unit temperature difference between the two junctions of a material is called its absolute TEP. Including this perturbation in the Boltzmann transport equation, the expression for TEP in bulk is given by [11]

$$S_b = -S\left(\frac{\partial \ln \sigma}{\partial E}\right)_{E=E_F} \quad (77)$$

where $S = \pi^2 k_B^2 T/3eE_F$. The physical size dependence of the TEP can be understood from that of the conductivity, σ. So, the TEP for thin films can be expressed as [72–74]

$$S_f = -S(V + U\beta_f/\beta_b) \quad (78)$$

where

$$V = \left(\frac{\mathrm{d}\ln A}{\mathrm{d}\ln E}\right)_{E=E_F} \qquad U = \left(\frac{\mathrm{d}\ln l_0}{\mathrm{d}\ln E}\right)_{E=E_F} \quad (79)$$

A is the area of the Fermi surface, E is the electron energy, E_F is the Fermi energy. The TEP is sensitive to the variation of Fermi surface area with respect to energy. Equation 78 indicates that a plot of S_f against β_f/β_b should be a straight line at any given temperature and the values of U and V can be obtained from the slope and intercept of such plots. Values of U and V can also be obtained

from resistivity measurements. The sign and value of the absolute TEP and the magnitudes of U and V provide information about the geometry of the Fermi surface. The validity of Equation 78 has been established in the FS model. This method of evaluating U and V using Equation 78 is valid for relatively thick films ($\lambda \gg 0.5$) and one has to be careful in interpreting experimental results in a thin film region since both U and V will vary with film thickness. Recently, Tellier *et al.* [75] have suggested an alternative method to determine U and V by studying the size and grain boundary effects in thin monocrystalline metal films. The TEP of the bulk metal is written as [11]

$$S_b = -S(U+V) \tag{80}$$

Using Equations 78 and 80 we can write

$$\Delta S' = S_f - S_b = SU - SU\rho_0/\rho_f \tag{81}$$

and

$$\frac{S_f}{S_b} = -\frac{S}{S_b}V - \frac{SU}{S_b}\left(\frac{\rho_0}{\rho_f}\right) \tag{82}$$

In the limit of large thickness, the resistivity ratio (ρ_0/ρ_f) in monocrystalline films approaches unity, and then a plot of S_f/S_b against ρ_0/ρ_f (using Equation 82) should yield a straight line with an ordinate intercept ($-SV/S_b$) and a slope of $-SU/S_b$. As S_b is a known quantity, one can easily determine U and V. Further, as the S_f/S_b and $\Delta S'$ against ρ_0/ρ_f plots should yield the same U value, one can evaluate V with a better accuracy. The expression for the TEP in the MS model for polycrystalline films is given by [72]

$$S_g = -S\left\{V + U\left[1 + \frac{g(\alpha)}{f(\alpha)}\right]\right\} \tag{83}$$

2.3.1. Pichard, Tosser and Tellier model

Recently, Pichard *et al.* [76] have proposed a general expression for the TEP of thin polycrystalline and monocrystalline films attached on a substrate, which includes correcting terms due to thermal expansion of the film and its substrate. The general expression of supported polycrystalline films is given by [76]

$$S_g = -S[V + U(1+X^*)] \tag{84}$$

Substituting Equation 72 into Equation 84 yields the most general equation for TEP:

$$S_g = -S\Big(V + \frac{U}{\beta_b}\{\beta_f - Y^*a_f - (X^* - Y^*)a_g - [2(\theta+1) + X^*(2\theta - n_f + 1) - Y^*(n_f+1)](a_s - a_f)(1-n_f)^{-1}\}\Big) \tag{85}$$

Equation 85 takes the following simple form if $a_f = a_s$ and $a_f = a_g$, and this equation was first proposed by Warkusz [77],

$$S_f = -S\left[V + U\frac{\beta_f + a_f}{\beta_b + a_f}\right] \tag{86}$$

Recently Pichard *et al.* [78] have taken into account the effect of the energy-dependent relaxation on the TEP. The relaxation time,

$$\tau = \tau_b E^z \tag{87}$$

where z takes positive or negative values and τ_b is the energy independent part of the relaxation time. Assuming negligible variation in any conduction parameters, the TEP is expressed as [78]

$$S_f = -S[V + (U^* + z)(\beta_f/\beta_b)] \tag{88}$$

where $U = U^* + z$. The size effect in the TEP vanishes for $z = -U^*$. The TEP due to free electrons (in the FS model) vanishes for $z = -\frac{1}{2}$, which is in agreement with the calculations of Verma and Jain [79]. It is suggested that whenever the electron relaxation time in a bulk material depends on electron energy, correlation even exists between the size effect of TEP and TCR of thin metal films.

It is worth noting that the MS model is essentially a one-dimensional model which is not suitable for analysing the transport phenomena occurring in a three-dimensional space. An alternative model of grain boundaries has been proposed by Warkusz [80, 81] but the mathematical framework has been questioned by Tellier and coworkers [82, 83]. In recent years, Tellier *et al.* [84] have proposed a statistical representation of grain boundaries by introducing an electronic transmission coefficient, ν, to express some average properties of the boundaries. These authors have developed an alternative expression for the resistivity [85] and TCR [86] in a three-dimensional conduction model and find excellent fit with the experimental data on zinc and aluminium films. It is important to note a

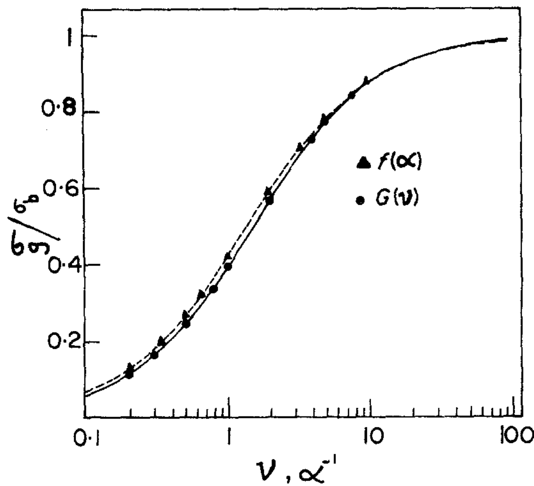

Figure 7 The reduced grain-boundary conductivity σ_g against ν and α^{-1} (after [85]).

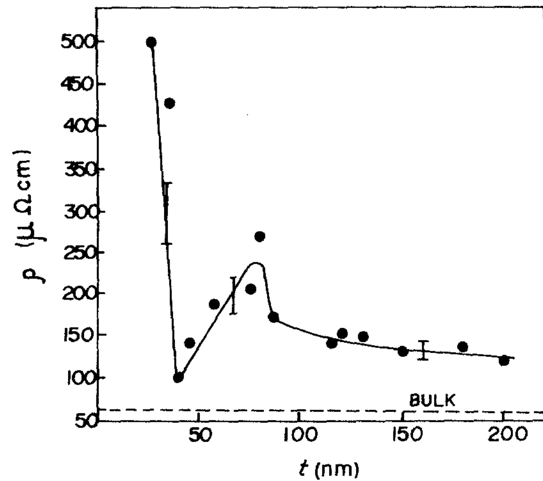

Figure 8 The dependence of resistivity ρ on the thickness of yttrium films deposited at 5×10^{-5} Pa. The vertical lines are error bars (after [89]).

remarkable similarity (Fig. 7) between the three-dimensional grain boundary curve and the MS curve. The deviation between these two curves is very small and the curves coincide when the observed boundary scattering is low.

3. Discussion of experimental results

3.1. Group IIIA elements

3.1.1. Scandium (Sc)

The electrical [86–88] and structural [86, 88] properties have been reported by Loboda *et al.* These authors have deposited scandium films in UHV conditions and have observed fcc phase (with lattice parameter from 0.476 to 0.48 nm) for very thin films ($t < 6$ nm) and hcp phase for higher thicknesses ($t > 9$ nm). These authors have also reported on the electrical resistivity of these films, and the results were analysed using the FS and MS models, assuming a diffuse scattering of the carriers ($p = 0$). Some of these results are given in Table I.

3.1.2. Yttrium (Y)

The electrical properties of yttrium films have been reported by many authors [89–93]. Recent experimental results [91–93] on the transport properties of yttrium films deposited at 10^{-4} Pa have been analysed using the FS model and these are given in Table I. Curzon and Singh [89] have reported an anomalous maximum in the thickness dependence of the resistivity curve (Fig. 8) around a film thickness of 75 nm, which is attributed to the formation of the dihydride of yttrium having lower resistivity than yttrium itself. It is rather surprising why the dihydride formation should be found only around $t = 75$ nm and not for other film thicknesses. They have also reported a sharp increase in the resistivity for low thicknesses (<40 nm) which has been ascribed to the oxide contamination of the films. However, no such anomalies have been reported by Angadi and Ashrit [92, 93]. It is, therefore, necessary to perform more experiments on yttrium films deposited in UHV conditions to resolve this anomaly in resistivity, since yttrium films are very susceptible to contamination from the residual gases. The TCR of yttrium films is reported [91] to be positive in the thickness range 10 to 80 nm. From the TCR data, $\beta\rho =$ constant, which shows that the Matthiessen' rule is valid for yttrium.

3.2. Group IVA elements

3.2.1. Titanium (Ti)

Transport properties of titanium films have been extensively investigated by many authors [94–104]. Titanium has been widely studied in thin film form for application as resistors, and in combination with its oxides as capacitors and other active devices [9].

Chander *et al.* [94] have reported measurements on the electrical properties of titanium films in the thickness range 7.5 to 35 nm. On heat-treating these films in different atmospheres they find an irreversible increase in resistivity on first heating from 20 to 200° C. These authors have also reported a negative TCR for smaller film thicknesses (<25 nm) and zero TCR for higher

TABLE I

Metal	Film thickness t (nm)	Deposition technique	Vacuum (Pa)	Substrate material	Substrate temp. (° C)	Dep. rate (nm sec^{-1})	Bulk resistivity ρ_b ($\mu\Omega$ cm)	ITFR ρ_∞ ($\mu\Omega$ cm)	TCR (deg C^{-1})	TEP (μV deg C^{-1})	m.f.p. l_0 (nm)	SP P	GBRC R	Film state	Film structure	References
Sc	30–280	Ev.	10^{-6}	(001) NaCl	RT	0.1–0.6	55	150			40	0	0.1–0.3		fcc and hcp	[86–88]
Y	9–100	Ev.	10^{-4}–10^{-5}	Glass	RT	0.3	57	65	0.0023		28.5	0.1		PC		[91–95]
Ti	7–1200	Ev.	10^{-6}	Glass	RT	35	43.1	58	0.027		28.5			PC	hcp	[95]
	300	Ev.	10^{-6}	Glass	RT	0.3		58	0.0036		28.5					[103]
	400–1390	Ev.	4×10^{-7}	SC mica	420	0.07		42.5						SC		[100]
Zr	11–1400	Ev.	10^{-6}			5	42.4	108.6	0.036						hcp	[95]
Hf	20–1500	Ev.	10^{-6}				30.6	61.7	0.067							[95]
		Sp.						50.0	0.0158							[105]
Va	5–50	Ev.	10^{-5}			8	19.9	31.0			1.13					[117]
Nb	10–100	Sp.	2×10^{-5}			0.15	14.5	39.5	0.0023						bcc	[120]
Ta	100	Sp.	6×10^{-4}		RT	35	13.1	230	−0.0002	−0.9– +1.5					fcc	[136]
Cr	~10	Ev.	10^{-7}			0.1–0.2	13	30	0.0011		50	0				[148]
	5–80	Ev.	10^{-4}	Glass	RT	0.1		50	0.0001	11.3	15.8	0.03		PC		[149, 153]
	10–120	Ev.	10^{-7}	Glass	300	0.2–2					4–14					[141]
Mo	5–160	Sp.	10^{-5}			0.1–0.2	5.7	6			39.5		0.44			[162, 163]
		Ev.	10^{-5}			3		9					0.41			[161]
W	170–270	Sp.		SiO_2 and Si		0.13–0.16	5.51	25–40	0.0012		10	0				[169, 170]
Mn	10–120	Ev.	10^{-4}	Glass, mica		0.2	185	376	0.00003	+0.8	96.7	0.35	0.09	PC		[177–179, 182]
Re	10–200	Ev.	10^{-6}	Quartz, sapphire		0.3	18.6	23.8			25.8	0			hcp	[187]
Rh	2–30	Ev.	10^{-4}	Glass	350	1.0	4.78	80								[188]
	30–200	Ev.	5×10^{-5}	Glass		0.4		4.93	0.00428		33.8	0		PC		[189]
Co	28–160	Ev.	10^{-4}	Glass		0.2–1.0	5.8	93.0	0.0009		36.5	0	0.0698	PC	fcc	[201, 202]
Ni	10–100	Ev.	10^{-4}	Glass			6.9	18.84	0.00086		18	0				[217]
	4	Ev.	4×10^{-4}	Mica		0.05					20	0.35				[218]
	10–1000	Ev.	10^{-4}	Glass	160	1.5					12.7	0	0.98	PC		[216]
	6–70	Ev.	10^{-4}	Glass				19.0	0.0023		16.4	0	0.18	PC		[219]
	10–40	Ev.	10^{-4}	Mica	420	2–6		8–12	0.0049		50.0	0.5				[209]
Pd	2–25	Ev.	10^{-4}	Glass	RT	0.14	10.8	11.2	0.0009	+10.35	25.5	0.3	0.05	PC		[227, 228, 233, 236]
	5–60	Ev.	2×10^{-8}	Glass	77 K			11.5	0.003	−9.3						[230, 231]
Pt	3	Ev.	10^{-7}	Glass		0.05–0.3	10.42	17.0			11.7	0.13				[244]
	3–300	Ev.	10^{-5}	Glass	300	0.8			0.0003			0.2				[243]

Note. Ev. – Evaporation; Sp. – Sputtering; RT – room temperature; ITFR – infinitely thick film resistivity; GBRC – grain boundary reflection coefficient; PC – polycrystalline; SC – single crystal; SP – specularity parameter.

thicknesses. A negative TCR in titanium films has also been reported by Singh and Surplice [101] for much lower thicknesses (5 to 6 nm), while they have reported a positive TCR for higher thicknesses. These authors have reported a bulk m.f.p. of 28.5 nm at room temperature, and this is in agreement with the m.f.p. values reported by other workers [95]. Titanium films exhibit small deviations from Mattheissen's rule [102]. This deviation is interpreted by the island or grain structure of the film and also by the gas adsorption on the grain boundary.

Friebertshauser and McCamont [95] have reported an exhaustive study on the electrical properties of titanium films from 1.5 to 300 K over a thickness range of 7 to 1200 nm as a function of different deposition parameters. The important results of this experimental report are summarized in Table I. The films deposited at lower substrate temperature (T_s) (< 400° C) are polycrystalline, while those deposited at higher T_s are monocrystalline in nature.

Recently Igasaki and Mitsuhashi [103] have reported the effect of T_s on the electrical properties of titanium films deposited under UHV conditions. These authors have also studied the structure, grain size and crystal orientation as a function of the T_s. These authors have concluded that grain size increases not only with increasing T_s during deposition, but also with annealing afterwards. The film resistivity decreases when

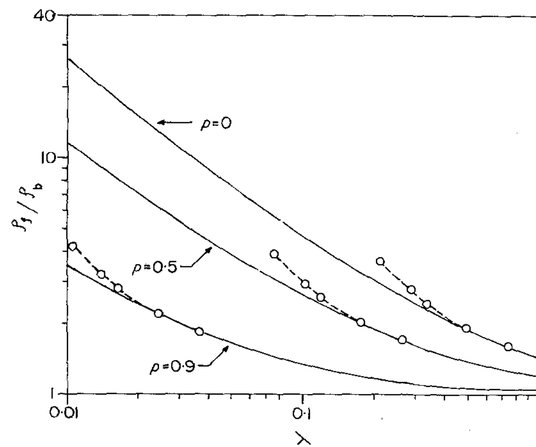

Figure 9 Reduced resistivity against reduced thickness λ at 4.2 K. Solid lines showing theoretical variation and broken lines showing experimental best fit for three values of $p = 0$, 0.5 and 0.9 are: $l_0 = 1850$ nm, $\rho_b = 0.4$ μΩ cm; $l_0 = 5230$ nm, $\rho_b = 0.38$ μΩ cm; $l_0 = 37600$ nm, $\rho_b = 0.35$ μΩ cm, respectively (after [100]).

deposited at higher T_s, which is primarily due to the differences in the grain size. It is rather surprising to note from their study that the TCR of these films remained independent of the T_s. It may be interesting to extend this study to very low thicknesses, and use the MS or Namba models to analyse the experimental results. Wawner and Lawless [96] have also reported the epitaxial growth of titanium films on NaCl substrates. These films exhibit the normal hcp phase for thicknesses > 50 nm and fcc phase for thicknesses less than 35 nm. Gould *et al.* [100] have also reported the epitaxial growth of titanium films in UHV conditions at a $T_s = 420°$ C. The important results are summarized in Table I. These authors have used FS theory to analyse their experimental results and have estimated infinitely thick film resistivity (ρ_∞) as 42.5 = μΩ cm, which is much lower than the polycrystalline values reported by other workers [95, 103]. These authors have found deviation between the FS theory and experimental results for small film thicknesses (Fig. 9).

3.2.2. Zirconium (Zr)

The only experimental study on the electrical properties of zirconium films has been reported by Friebertshauser and McComont [95]. The important results of this report are given in Table I.

3.2.3. Hafnium (Hf)

There are very few reports [95, 105–107] on the electrical properties of hafnium films. Most of these measurements are on films grown by sputtering. It is reported [106] that the film resistivity approaches the bulk value for films prepared by sputtering in pure argon. Some of these results are given in Table I.

3.3. Group VA elements

3.3.1. Vanadium (V)

There are some experimental results reported [108–118] on the transport properties of vanadium films. Most of these measurements have been carried out at liquid helium temperature. Chander *et al.* [109] have examined the size effect of these films at room temperature using the FS model and have reported electron m.f.p. values in the range 60 to 100 nm. Borodziuk-Kulpa *et al.* [117] have done a systematic study on the electrical properties of vanadium films and also studied the effect of annealing on the resistivity. The important results are shown in Table I. These

authors have used the modified MS equation proposed by Wedler and Wissmann (Equation 40) to analyse their experimental results. The decrease in film resistivity after annealing is attributed to the disappearance of structural defects which is also accompanied by an increase in the electron m.f.p. These values of m.f.p. are in reasonable agreement with those reported by other workers [108, 112].

3.3.2. Niobium (Nb)

One of the earliest attempts to grow high purity niobium films has been reported by Raiden and Furey [119]. However, very few reports [120–122] are found in the literature on the transport properties of thin niobium films. A systematic study on the electrical properties of niobium films has been published by Sosniak [120], and the important results are given in Table I. Ogawa *et al.* [121] have deposited niobium films on a glass substrate in the temperature range 77 to 300K. Reiche and Pompe [122] have investigated electrical properties of niobium films in the temperature 9 to 50K and in the thickness range 10 to 150nm. These authors have used the FS model to fit the experimental results. There is a considerable disagreement between the FS model and experimental data (Fig. 10), which appears quite strange since the FS model approximated by Equations 9 and 10 is valid for large thicknesses.

3.3.3. Tantalum (Ta)

Tantalum is one of the most widely studied [123–138] refractory metals in thin film form, in view of its applications in the fabrication of thin film devices [1]. Readers are referred to an excellent review by Baker [6] on the preparation and properties of tantalum films, and for literature prior to 1972.

Perinati and Piacentini [136] have studied transport properties of tantalum deposited by reactive r.f. sputtering in a vacuum of 6×10^{-4} Pa. These authors have investigated the effect of N_2 doping on the resistivity, TCR and TEP of 100 nm tantalum films. The important findings of this report are given in Table I. The resistivity of tantalum films is found to be in the range 170 to 30 000 $\mu\Omega$ cm, depending on the deposition conditions. The TCR and TEP are found to be in the range -0.0002 to $+0.0002$ deg C^{-1} and -0.9 to $+1.5$ μV deg C^{-1}, respectively [136]. The negative TCR and electrical conduction in very thin films has been explained [128] on the basis of an activated tunnelling mechanism. Electron microscope studies depict the presence of large metallic islands largely surrounded by amorphous Ta_2O_5 [137]. The wide variations in the physical and structural properties of tantalum films suggest that these films are very susceptible to deposition parameters.

3.4. Group VIA elements

3.4.1. Chromium (Cr)

Transport properties of chromium films have been reported by many authors [139–157]. The first systematic report on the electrical resistivity, TCR and structure of chromium films has been published by Gould [141]. These films were deposited at 10^{-7} and 10^{-4} Pa and at $T_s = 300$ and 20° C. The important results are given in Table I. The thickness dependence of resistivity and TCR are shown in Figs. 11 and 12, respectively. The TCR is negative for very thin films ($t < 20$ nm) deposited on substrates held at room temperature. Resistivity

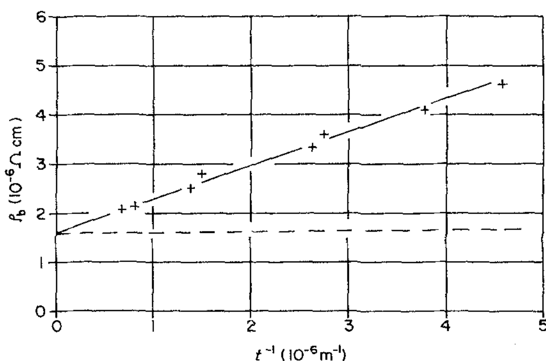

Figure 10 Dependence of resistivity of evaporated niobium films on thickness. (———) shows the experimental results; (– – – –) shows FS approximation (after [122]).

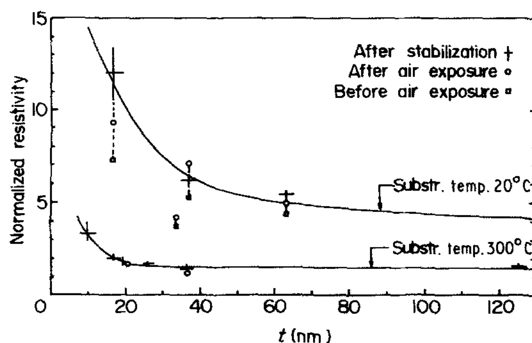

Figure 11 Normalized resistivity of chromium films deposited at 10^{-7} Pa for $T_s = 20$ and 300° C (after [141]).

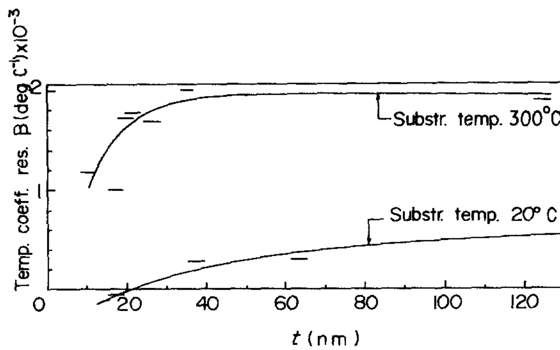

Figure 12 TCR of chromium films deposited at 10^{-7} Pa for T_s = 20 and 300° C (after [141]).

of thick films deposited at T_s = 300° C was found to be 50% higher than the bulk value of chromium. Gould has also reported that films deposited at higher rates (2 nm sec^{-1}) and T_s = 22° C exhibit lower resistivities and higher TCR for thick films. However, films deposited at T_s = 300° C do not show this dependence at higher deposition rates.

Sanchez *et al.* [148] have studied electrical properties of chromium films grown in UHV (10^{-7} Pa) conditions on glass substrates at different T_s ranging from 50 to 320° C. The important results are given in Table I. High electrical resistivity and negative TCR in chromium films has also been confirmed by many authors [149–151]. It is reported [144, 146] that a negative TCR is caused by a small amount of amorphous oxide (Cr_2O_3). Chromium films become amorphous when deposited on substrates held at 4.2 K [142, 152]. The reversible variation of resistance as a function of temperature of both amorphous and crystalline chromium films reveal a negative TCR. The irreversible resistance drop observed in chromium films at 250 to 320 K is connected with the phase transition of chromium films from antiferromagnetic state to paramagnetic state. A similar transition region in the TCR data has also been reported by Gould [141]. It is reported that chromium film resistivity decreases when overcoated with insulating films [143]. The effect is explained as being due to a change in the surface tension of the metallic films. It is, however, interesting to note [147] that the deposition of SiO or a cermet layer on chromium films leads to an increase in the number of electrons passing into the substrate and hence to an increase in activation energy and work function increment. This demonstrates the role of substrate-assisted tunnelling in discontinuous chromium films which exhibit a negative TCR. Imura [150, 156] has critically studied the effect of deposition parameters on the electrical and structural properties of chromium films and has concluded that the three structural forms: amorphous, crystalline and their co-existence depends on T_s and deposition rate.

Thermopower measurements on chromium films have been reported by Angadi and Udachan [153] in the thickness range 10 to 100 nm. They have used the FS model to estimate infinitely thick film (TEP (S_∞) as 11.3 μV deg C^{-1}. This value compares very well with the TEP value (12 μV deg C^{-1}) reported for bulk chromium [157]. It is interesting to note from Fig. 13 that the TEP is negative for low thicknesses and positive for high thickness films. Angadi and Udachan [151, 154, 155] have also investigated the effect of T_s, d.c. and a.c. fields on the electrical resistivity of thin chromium films.

3.4.2. Molybdenum (Mo)

Although molybdenum films have become of special interest as self-aligned gates and interconnection materials accompanying the fast progress in LSI technology, there are only a few reports [158–165] on their transport properties. One of the earliest reports on molybdenum films is due to Degenhart [158]. Oikawa [161] has reported electrical resistivity of molybdenum films evaporated by an electron beam gun. The resistivity is found to be influenced by T_s and independent of thickness after 100 nm (Fig. 14). The film resistivity decreases on annealing at 700° C. The resistivity is assumed to be due to grain-boundary

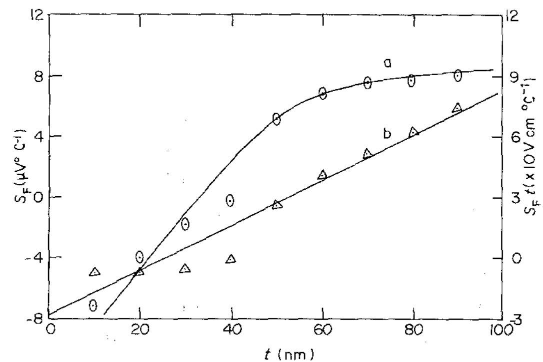

Figure 13 Thickness dependence of TEP for chromium films. Curve a shows a plot of thermopower (S_F) against thickness t (experimental points are shown by ○, curve b shows a plot of $S_F t$ against t for chromium films (experimental points are shown by △) (after [153]).

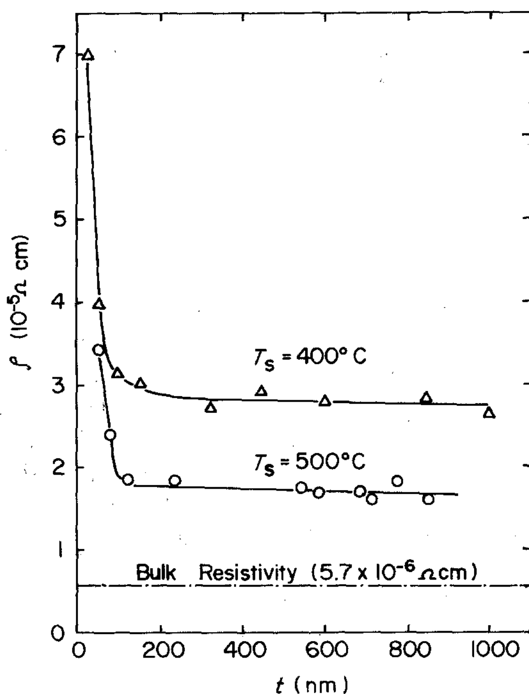

Figure 14 Electrical resistivity against thickness relation for 400 and 500° C substrate temperature T_s during deposition. Deposition rate and total pressure at deposition were 3 nm sec^{-1} and 7 to 9 × 10^{-5} Pa, respectively (after [161]).

scattering. The reflection coefficient, R, is found to be dependent on T_s. Some of these experimental results are summarized in Table I. It is interesting to note that resistivity is independent of deposition rate in the range 1 to 6 nm sec^{-1}. Oikawa has used MS theory to analyse the experimental results. It is reported that resistivity of molybdenum films is mainly dominated by the grain-boundary scattering of the conduction electrons and that the reflection coefficient, R, of conduction electrons is determined by the oxygen content in the grain boundary. It is reported [162] from the annealing behaviour of molybdenum films that the grain growth is quite drastic at annealing temperatures higher than 900° C.

However, in the case of sputtered molybdenum films [163], the electrical resistivity within the individual grains is 6 μΩ cm at 25° C and is independent of the sputtering conditions or annealing temperature upto 900° C. This value is quite close to the value of the electrical resistivity of bulk molybdenum. This shows that the isotropic back ground scattering for sputtered molybdenum is assumed to be similar to that of bulk molybdenum. The scattering at the surfaces is related to the surface roughness and increases after annealing. The decrease in film resistivity after annealing, when the film thickness is sufficient to ignore the surface scattering effect, is caused by a decrease in the scattering at the grain boundaries for zero bias sputtered films and by an increase in the grain diameter for r.f. bias sputtered films.

3.4.3. Tungsten (W)

There are not many published reports [166–171] on the transport properties of tungsten films. Chopra *et al.* [167] have published a first systematic report on thin tungsten films by ion-beam sputtering. The films were deposited on substrates of glass, rock-salt and mica at a temperature of 250 to 400° C. The fcc phase was found to transform slowly to bcc phase at 700° C.

Dobson and Hopkins [168] have reported electrical conductivity measurements on tungsten films deposited on Pyrax glass substrate cooled to 90 K, under UHV conditions. Films are found to be discontinuous below 3 nm. These authors have provided a qualitative explanation of their results based on thermionic emission of carriers.

Sheng *et al.* [169] have controlled electrical resistivity in the range 7 to 100 μΩ cm by a proper choice of T_s, gas ambient and substrate bias. These authors have observed β–tungsten phase in a few of the high resistivity tungsten films. Important results are high-lighted in Table I. Annealing of tungsten films produces a significant change in the defect structure of the film. As-deposited grains contain a large concentration of crystal defects which are removed out after heat-treatment at 900 to 1000° C. The surface texture changed to smooth on annealing, and this produced a lowering of resistivity due to a greater degree of specular reflection of electrons.

Petroff and Reed [170] have studied the electrical resistivity of β-tungsten films in the temperature range 1.4 to 900 K. The TCR is found to vary from negative to positive values with decreasing amount of β-tungsten in the film. These authors have also reported an irreversible phase transformation from β-tungsten to α-tungsten at 400 K or above. The occurrence of a new phase is also reported which forms reversibly below 300 K and is identified as WO_3 from TEM studies.

3.5. Group VIIA elements

3.5.1. Manganese (Mn)

In recent years, transport properties of manganese

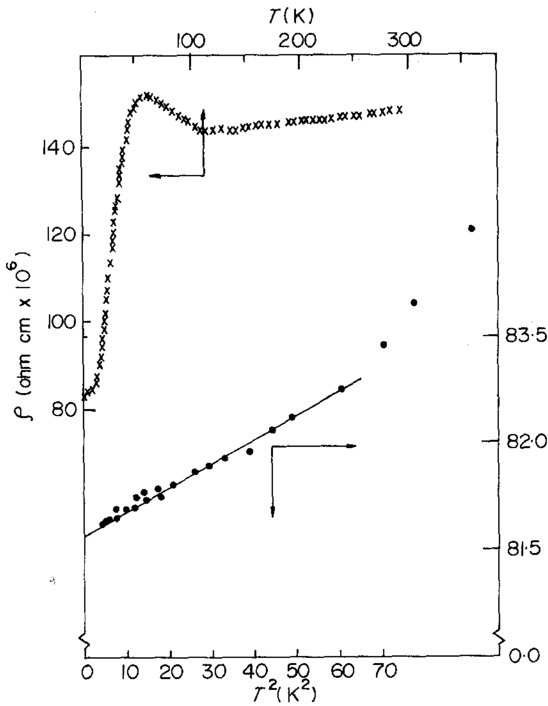

Figure 15 Temperature variation of resistivity of "normal" manganese films showing T^2 dependence (after [172]).

films have attracted the attention of many workers [172–182]. Grassie and Adanu [172] and Grassie and Boakye [173] were the first to report on the anomalous low temperature dependence of resistivity in manganese films. These authors find some similarity between their data and those of bulk α-manganese alloys with cobalt and nickel impurities. The zero temperature resistivity of the film is appreciably higher than the bulk, being of the order of $80\,\mu\Omega$ cm in comparison with $7\,\mu\Omega$ cm, and the temperature dependence of the resistivity at low temperature is T^2 (Fig. 15). This anomalous low temperature resistivity in manganese films is attributed to the local inhomogeneities or strains associated with the deposition process which prevents manganese atoms from occupying exactly the same configuration as that of bulk crystals. The electronic configuration of the misplaced atoms would be critically dependent on the local environment and may generate spin fluctuations similar to a transition element impurity atom. The excess low temperature resistivity increases as the perfection of the film decreases. It is also suggested [173] that the m.f.p. of these high resistivity α-Mn films cannot be more than 0.133 nm.

In recent years, Angadi and Shivaprasad [177–182] have done an exhaustive study on the electrical resistivity, TCR and TEP of manganese films. These results are given in Table I. These authors have also studied electrical resistivity in the temperature range 77 to 460 K [182] (Fig. 16). The resistivity increases as the temperature is lowered for lower thicknesses, while it remains unaffected at higher thicknesses (>40 nm). The resistivity of these films is strongly dependent on the deposition parameters [180, 181]. These authors have also measured the TEP of manganese films [182] in the temperature range 25 to 150° C. The manganese films exhibit extremely small TEP ($-0.8\,\mu$V deg C^{-1}), and this value is much smaller than lead ($-1.3\,\mu$V deg C^{-1}), which is often used as a reference material in the fabrication of thin film thermoelectric junctions. The fact that thin manganese films exhibit large resistivity, very low TCR and TEP renders them suitable for use in the fabrication of thin film resistors.

3.5.2. Rhenium (Re)

There are very few experimental reports [183–187] on the transport properties of rhenium films. An exhaustive report on the electrical properties of rhenium films was recently published by Ul Haq and Meyer [187]. They have studied electrical properties of rhenium single-crystal films prepared by electron bean evaporation at 10^{-6} Pa on polished single-crystal sapphire substrates at various T_s. These results are summarized in Table I. These authors have also studied the influence of deposition parameters like evaporation rate, pressure, substrate material and substrate temperature on the electrical properties of these films.

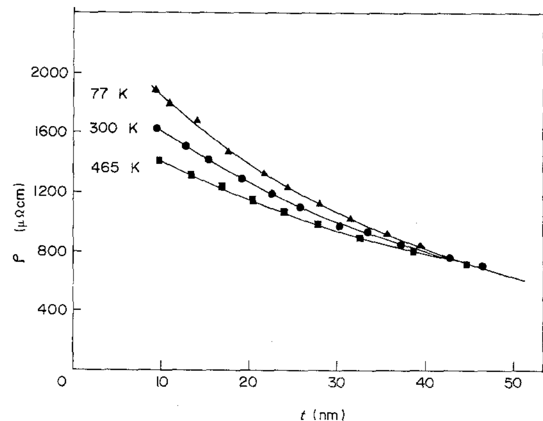

Figure 16 Thickness dependence of resistivity of manganese films measured at three temperatures: 77, 300 and 465 K (after [182]).

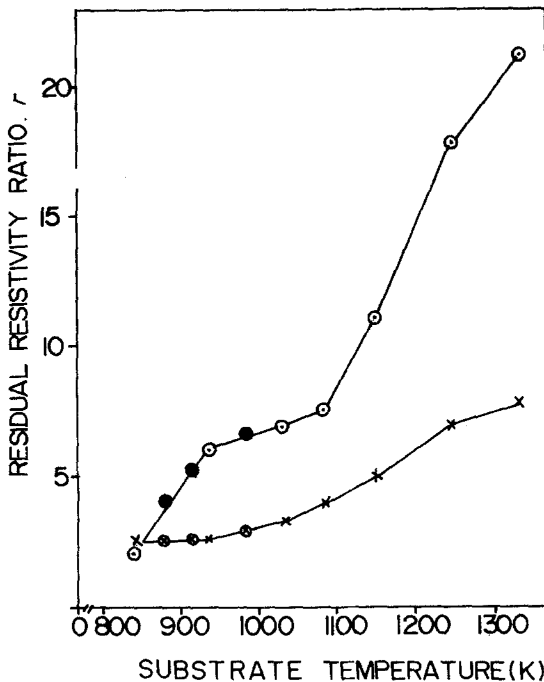

Figure 17 Residual resistivity ratio of rhenium films 100 nm thick grown on polished (o, •) and rough (X, o) substrates as a function of substrate temperature (after [187]).

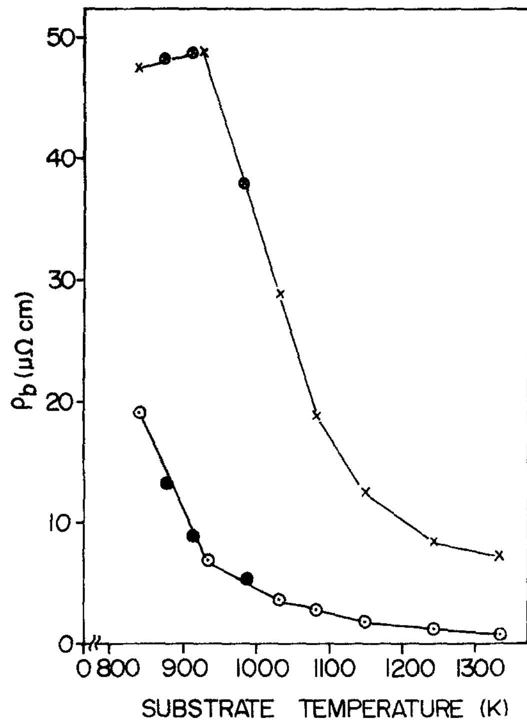

Figure 18 Residual resistivity ρ_b as a function of T_s for rhenium films grown on polished (o, •) and rough (o, X) substrates ($t \approx 100$ nm) (after [187]).

They have concluded that the variation of deposition rate and pressure in the ranges 0.1 to 2 nm sec^{-1} and 10^{-3} to 10^{-6} Pa, respectively, has little effect on resistivity and structure of rhenium films. However, they have reported a strong influence of the substrate material (Fig. 17) on the elastic strains in rhenium films. Increase in the T_s improved considerably the film quality and decreased the film resistivity (Fig. 18). The experimental results of rhenium are analysed using the FS model. Dimitriev *et al.* [186] have determined a value of $14.3 \times 10^{-11}\,\Omega\,cm^2$ for the product of ρl_0 and a p value of 0.8. This value is a factor of 3.2 larger than that reported by Ul Haq and Meyer [187]. This discrepancy may be due to the fact that the films deposited by Dimitriev *et al.* [186] had very high resistivities, possibly due to the presence of a metastable phase of rhenium.

3.6. Group VIIIA elements

3.6.1. Rhodium (Rh)

Transport properties of rhodium films have attracted the attention of only a few authors [188, 189]. Hoffman and Coutts [188] have evaporated rhodium films in 10^{-4} Pa vacuum, on glass substrates. Very thin films have exhibited isolated island structure with high resistivity values. When the film thickness increases to 30 nm, continuous films have been observed.

A systematic study on the electrical resistivity and TCR of rhodium films has been reported by Koshy [189]. The important results are summarized in Table I. This author has used the FS model to analyse experimental results. The thickness dependence of resistivity for different temperatures is shown in Fig. 19.

3.6.2. Iron (Fe)

There are very few reports published on the transport properties of iron films [190–194] and most of these are on amorphous films.

3.6.3. Cobalt (Co)

Savornin [195] reported the first experimental measurements on the electrical properties of cobalt films. His results are found to be in agreement with the FS model, indicating complete diffuse scattering (i.e. $p = 0$). On the other hand, Mola and co-workers [196, 197] have explained their observations in the light of the MS model

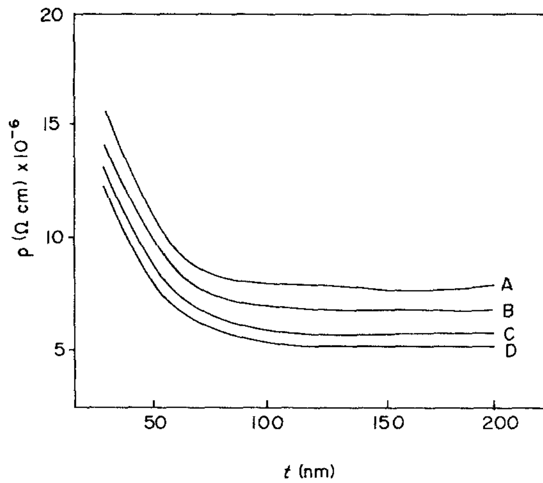

Figure 19 The resistivity of rhodium films as a function of film thickness for different temperatures: A, 150° C; B, 100° C; C, 50° C; D, 20° C (after [189]).

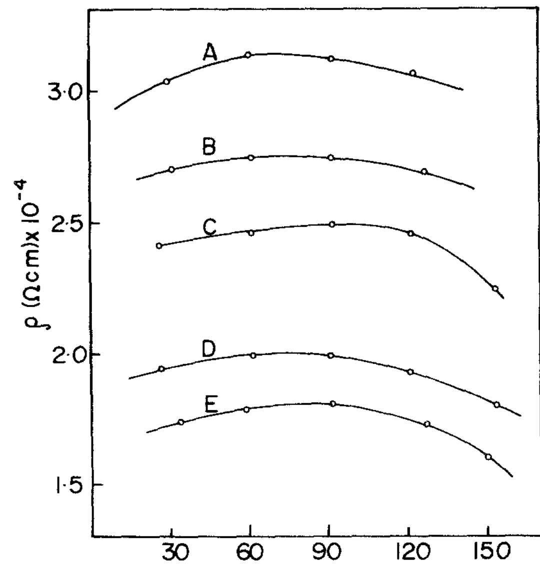

Figure 20 The resistivities of cobalt films as a function of temperature (after [202]).

with grain-boundary reflection coefficient, R, ranging from 0.1 to 0.5, and found it to be thickness dependent. The growth of cobalt films was studied by Fisher and Tayler [198], and they have concluded that the growth pattern of cobalt films was similar to other ferromagnetic films and that magnetic forces play an important role in the film structure.

For cobalt films prepared by evaporation technique, the film structure is dependent on T_s [195, 198–201, 203, 204]. Different workers in this field have observed a metastable fcc phase when deposited around room temperature. Although the fcc phase is the high temperature bulk phase, it is often retained at room temperature, because the free energy difference between the two phases is rather small. With increasing T_s, mixed fcc and hcp phases were generally observed [201].

Pal *et al.* [202] have recently reported a systematic study on the electrical resistivity and TCR of cobalt films. The important results are given in Table I. The resistivity of cobalt films deposited at room temperature is shown as a function of temperature in Fig. 20 and the annealing effect is shown in Fig. 21. Cobalt films behave reversibly and show a positive TCR [202] over the entire range of thickness. It is reported that the FS model with $p = 0$ reproduces the experimental results satisfactorily. The values of m.f.p. reported by Pal *et al.* [202] are somewhat larger ($l_0 = 49$ nm) than those obtained by Van Gurp [201] ($l_0 =$ 36.5 nm) and Savornin [195] ($l_0 = 13$ nm). The above disagreement on m.f.p. values reported by different workers is probably caused by the severe limitation of the FS model used to analyse these results. Pal *et al.* have also used the MS model to fit their results and according to these authors the agreement is satisfactory for $D = 36$ nm, $R = 0.07$ and $p = 0$. The theoretical and the experimental

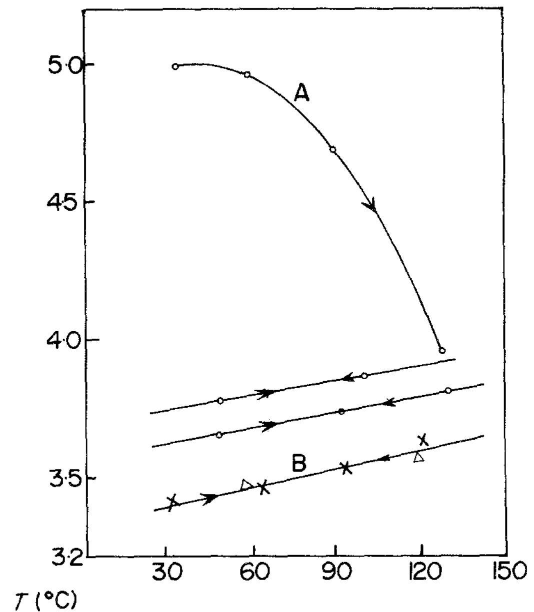

Figure 21 The effect of annealing and thermal cycling on the resistivity of cobalt films deposited at room temperature (after [202]).

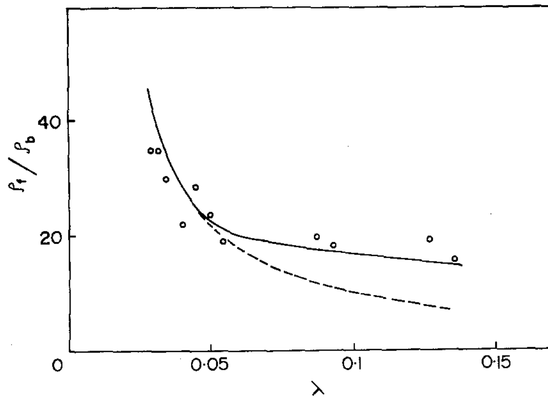

Figure 22 Comparison of the experimental observations for cobalt films with a MS curve. ○ experimental points; ——— MS curve with $D = 36$ nm, $R = 0.0698$, $p = 0$; ---- MS curve with $D =$ film thickness, $R = 0.698$, $p = 0$ (after [202]).

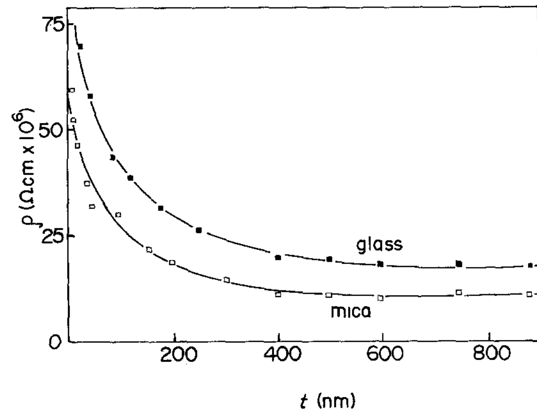

Figure 23 Resistivity against thickness at room temperature, *in situ* for non-annealed nickel films thermally evaporated at 10^{-4} Pa on mica and smooth glass at 160° C (after [216]).

curves deviate considerably beyond 36 nm if the grain size is considered equal to the thickness of the film (Fig. 22). The assumption that the grain size should always be equal to the thickness of the film, to interpret experimental results, using the MS model has been questioned by Van Gurp [201].

3.6.4. Nickel (Ni)

Electrical properties of nickel films have been reported by several authors [205–220]. Kleefeld and Hirsch [208] have reported the epitaxial growth of nickel films on rock-salt substrates heated upto 500° C. Verma [209] has reported electrical resistivity measurements on epitaxial nickel films. Resistivity and TCR measurements are found to follow FS theory for $p = 0.5$, taking $l_0 = 50$ nm. Verma [209] has also tried to explain the lower values of TCR on the basis of thermally induced strains but the effect is found to be too small to account for the observed deviation in $d\rho/dT$. The observed thickness dependence of resistivity values at 77 K shows only little influence of geometrical size effect in the thickness range 40 to 110 nm [212].

Eid *et al.* [216] have recently reported on the size-dependent electrical conduction in nickel films over a wide thickness range of 10 to 1000 nm. The effect of annealing on the electrical resistivity and TCR of these films has also been reported by these authors. The TCR was found to be negative for the non-annealed films of island structure and positive for the annealed ones. The resistivity of the film decreased after annealing. These authors have used the FS and MS models to analyse their experimental results and some of these results are summarized in Table I. The estimated values of ρ_∞ and l_0 are in agreement with values reported by other workers [205, 214, 217]. The abrupt increase in resistivity for thinner films (<30 nm) is attributed to the discontinuous structure of films and conduction by tunnelling [205]. The large reduction in resistivity on annealing is mainly due to increasing island size and reducing island separation due to coalescence during the annealing process. It is interesting to note the reduction in resistivity of continuous films deposited on glass (90%) (Fig. 23) is due to the epitaxial growth, which is preferable on mica.

Pal and co-workers [213, 217] have reported electrical resistivity and TCR measurements on nickel films deposited at 10^{-4} Pa in the thickness range 10 to 80 nm. Films deposited at room temperature show an irreversible behaviour when subjected to thermal cycling followed by annealing, which is attributed to inherent defects and agglomeration. However, films deposited at 150° C show reversible behaviour within the experimental range of temperature. Fig. 24 shows the thickness dependence of resistivity and TCR for films deposited at 150° C. The TCR was positive for thickness upto 14 nm. It is generally concluded by these authors [213] that reproducible results are obtained only if either the deposition temperature exceeds the Curie temperature or the film is annealed above the Curie temperature. It is also reported [144] that the TCR changes from positive to negative values at about 5×10^{-3} Pa

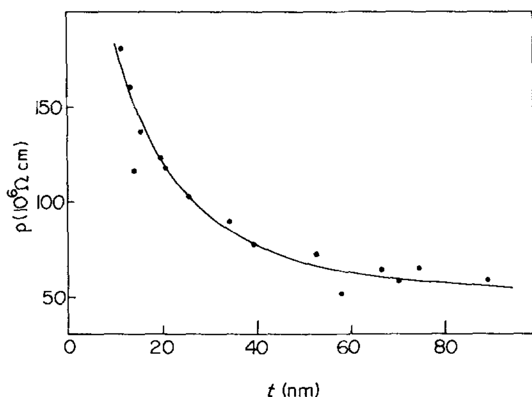

Figure 24 Resistivity of nickel films as a function of thickness (after [217]).

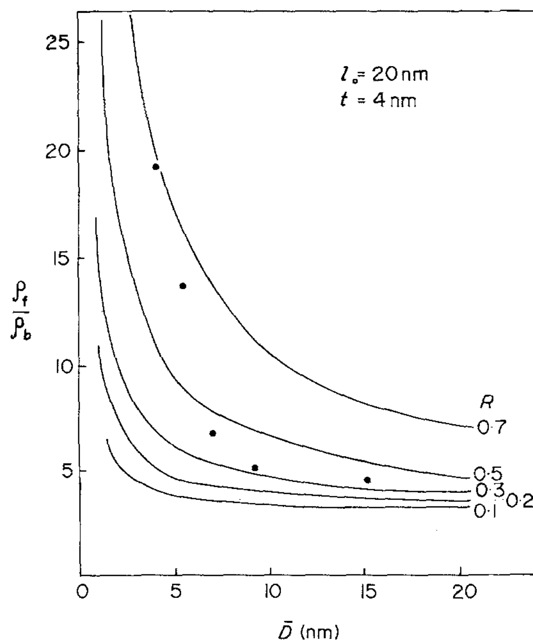

Figure 25 Theoretical and experimental dependence of ρ_f/ρ_b on the mean grain size $\bar{D}$ for film thickness t = 4 nm and several values of R (curves ——— MS theory; • -experimental points (after [218]).

when nickel films are deposited in the presence of oxygen.

Stary and Sefcik [218] have studied the effect of annealing in hydrogen atmosphere on the grain size of nickel films. The grain size was measured directly by TEM. From Arrhenius plots these authors have determined the activation energy of grain growth as 0.25 eV and this is found to be low in comparison with that reported for bulk nickel. This is attributed to the proximity of surfaces which influence grain growth very appreciably. These authors have used the MS model to compare film resistivity for different grain sizes. The results are given in Table I and shown in Fig. 25.

Angadi and Udachan [219] have also reported electrical resistivity and TCR of nickel in the thickness range 6 to 70 nm and the results are analysed using the FS and MS theories. Values of p, l_0 and R are in agreement with those reported by other workers [217, 218]. These authors have reported that $\beta\rho$ is constant, indicating that Matthiessen's rule is valid in nickel films.

Le Bas [207] has observed an increase in resistivity and TCR of very thin films of nickel when an electric field is applied parallel to the substrate during the deposition, and this is attributed to the increase in the size of small islands.

3.6.5. Palladium (Pd)

There are several experimental reports [221–236] on the transport properties of palladium films. Real [221] has reported the TEP of palladium films, vacuum deposited by electron bombardment on glass substrate at 200° C and 10^{-4} Pa and subsequently annealed in air at 400° C for 2 h.

Antonangeli *et al.* [226] have studied the influence of hydrogen on the electrical resistivity of palladium films. The changes in resistance due to hydrogenation are quite different in films compared to those of bulk samples. These experimental results suggest that H_2 induced readjustment of crystal structure takes place when hydrogen diffuses in palladium. The maximum equilibrium concentration of H_2 obtainable in these films is lower than in the bulk samples.

Wedler and co-workers [230, 231] have recently reported on the electrical resistivity and TCR of annealed and unannealed evaporated palladium films. Depending on the film thickness, the high temperature annealing was done at the temperature where the film showed a minimum resistance. These authors have observed that palladium films annealed at the temperature of minimum resistance exhibit a reversible behaviour in their physical properties at low temperatures. The transport properties have been analysed using the FS and MS models and these are given in Table I. The thickness dependence of resistivity has been studied under different measuring and annealing conditions (Fig. 26). The films show minimum resistance when annealed at high temperatures (>400 K).

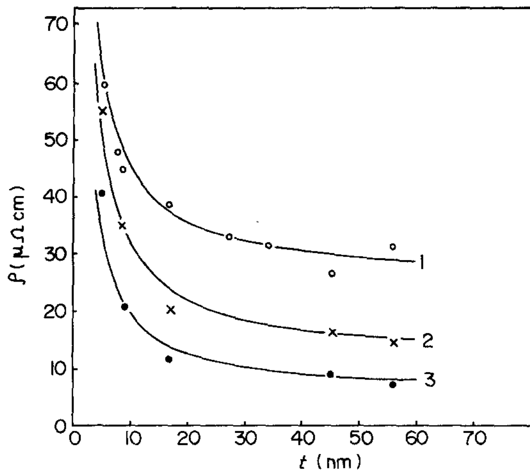

Figure 26 The thickness dependence of the resistivity ρ of evaporated palladium films: curve 1, measuring temp. = 80 K, annealing temp. = 80 K; curve 2, measuring temp. = 280 K, annealing temp. = 400 K; curve 3, measuring temp. = 80 K, annealing temp. = 400 K (after [231]).

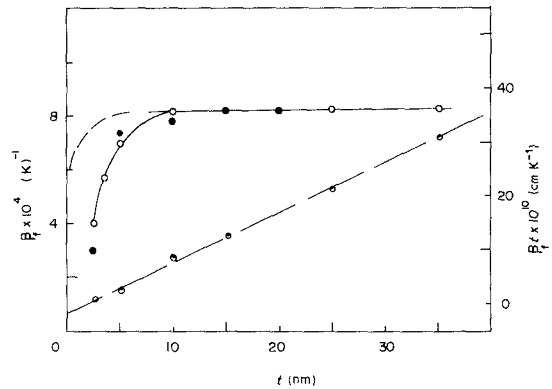

Figure 28 Thickness dependence of TCR of palladium films. Experimental points shown by ○ are measured in the temperature range 300 to 465 K, and those measured in the range 77 to 300 K are represented as ●. The dashed and the continuous curves are due to FS and MS models, respectively. The βt against t is the dashed straight line (after [228]).

Angadi and Shivaprasad have done an extensive investigation on the electrical resistivity [227], TCR [228] and TEP [233]. These authors have also reported recently the effect of deposition parameters on these transport properties [233, 235, 236]. Experimental results are in agreement with the FS and MS theories for higher and lower thicknesses, respectively. The important results are given in Table I. The thickness dependence of resistivity and TCR are shown in Figs. 27 and 28, respectively. For very thin films, the resistivity is markedly high, but for higher thicknesses it approaches a constant value. The TCR of palladium exhibits a size effect for lower film thicknesses (< 10 nm). The TCR is reported to be positive for all thicknesses. These authors have verified that Matthiessen's rule is valid in palladium films. TEP of palladium ($10.5\,\mu$V deg C^{-1}) is reported [233] to be positive over the entire thickness range (2.5 to 25 nm) and is in agreement with the bulk value [157]. However, Wedler and co-workers [230, 231] have reported a negative value of TEP for palladium films. These authors have also reported a decrease in TEP value with increase in thickness (Fig. 29). The difference in growth conditions and temperature range of measurements might have caused this discrepancy. Wedler and co-workers have deposited palladium films at 77 K (10^{-8} Pa) and annealed at 300 K, while Angadi *et al.* have deposited these films at 300 K (10^{-4} Pa) and

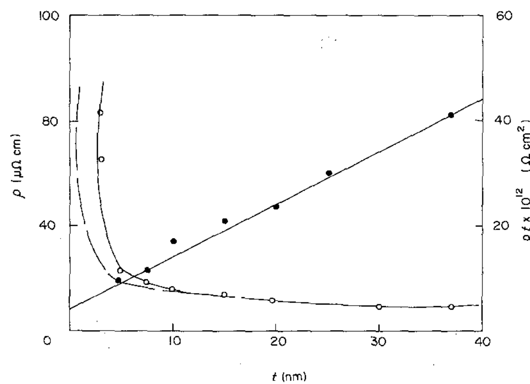

Figure 27 Thickness variation of the electrical resistivity of evaporated palladium films. The dashed and continuous curves are due to the FS and MS models, respectively. Data points of ρt against t graph are shown by ● (after [227]).

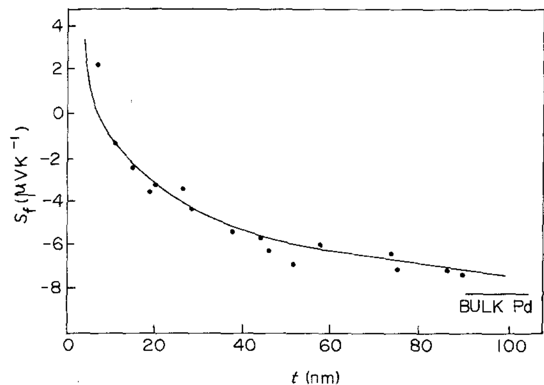

Figure 29 The thermoelectric power S_f as a function of thickness t at 273 K for palladium films (after [230]).

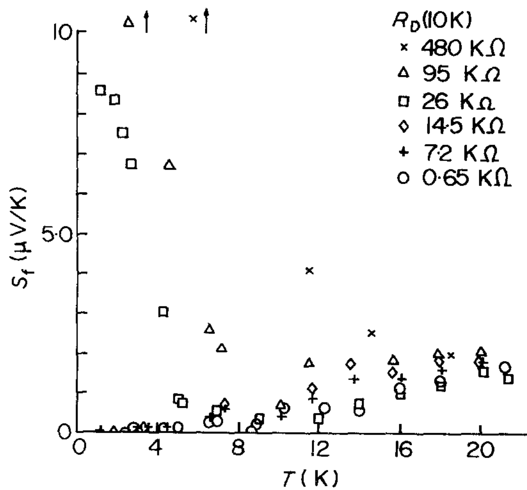

Figure 30 Absolute thermopower as a function of temperature for palladium films. Samples with $R_\square < 30\,\mathrm{k\Omega}\,\square^{-1}$ show metallic behaviour. Samples with $R_\square \gtrsim 30\,\mathrm{k\Omega}\,\square^{-1}$ show the presence of an energy gap (after [237]).

annealed at 423 K. The annealing temperature and TEP measuring temperature range determine the defect composition of the films, and thus their absolute TEP values. Wedler and Chander [231] have also reported a positive value of TEP in ultra-thin (<20 nm) palladium films. It is reported [231] that a decrease in thickness and an increase in the density of defects may cause the resistivity to increase and the TEP to become positive.

Recently, Burns *et al.* [237] have studied TEP in ultra-thin films of palladium (1.8–2.5 nm) at low temperatures (1 to 25 K). Fig. 30 shows the absolute TEP as a function of temperature. The reported TEP values are much smaller than the bulk values. Higher resistivity films show larger low temperature TEP and deviate from metallic behaviour at higher temperature. These authors have used a localization model [238] to analyse their results and show that $S \sim T^{1/3}$ for the two-dimensional case. They have concluded that for low-resistivity palladium films, TEP shows a metallic behaviour with $S \rightarrow 0$ as $T \rightarrow 0$.

3.6.6. Platinum (Pt)

Transport properties of platinum films are investigated by a few authors [17, 239–244]. Van Steensel [17] has reported electrical conduction in platinum films, vacuum deposited on insulating substrates of quartz glass and barium titanate. The film shows a negative TCR and this is due to the island structure of these films. The temperature dependence of conductance in these films gives an activation energy for platinum films in the range 0.088 to 0.125 eV. According to Steensel, thermionic emission is the important conduction mechanism for very thin platinum films, although it does not completely explain all the experimental results.

Several years ago, Jaunet *et al.* [239] reported the epitaxial growth of platinum films on NaCl and CaF_2 substrates at $T_s = 400$ and 670° C respectively. Misek [240] has reported the electrical resistivity of thin platinum wires (0.02 to 0.4 mm) and has used the FS model to analyse the results with $p = 0$. The m.f.p. of electrons at 4.2 K is found to be 0.05 mm. Heras [242] has determined the m.f.p. of platinum films by a graphical and iterative method. The temperature dependence of the m.f.p. of electrons between 77 and 673 K is found to be proportional to $T^{-3/2}$.

Recently Hoffman and co-workers [243, 244] have reported a systematic study on thin and very thin films of platinum. The important results are given in Table I. The results are in good agreement with the FS theory for film thicknesses greater than 10 nm (Fig. 31). The *in-situ* measurements show strong dependence on the evaporation condition, e.g. evaporation rate, substrate temperature and substrate properties. According to these authors, very thin films (<2 nm) do not exhibit island structure and ohmic conductivity is observed for film thicknesses as low as 0.5 nm, which is quite contrary to what is reported by Steensel [17]. The discrepancy between the FS model and experimental results for low thicknesses (<10 nm) has been explained qualitatively using the Namba model (Fig. 32). These authors have tried to fit their data with $p = 0$ and $h = 0.31$ nm. The surface roughness, h, has been found to be dependent on the evaporation rate. Higher evaporation rates produce smaller surface roughness. These authors have also tried to fit their data with $h \neq 0$ and $p = 0$ and were not successful, and this suggests that a certain amount of specularity ($p \neq 0$) is necessary. Fig. 33 shows the thickness dependence of the conductivity based on the FS and Namba models. Excellent fit with the experimental data is obtained using the Namba model at very low thicknesses.

4. General comments on the experimental results

Based on our review of the experimental results on the electrical resistivity, TCR and TEP of transition

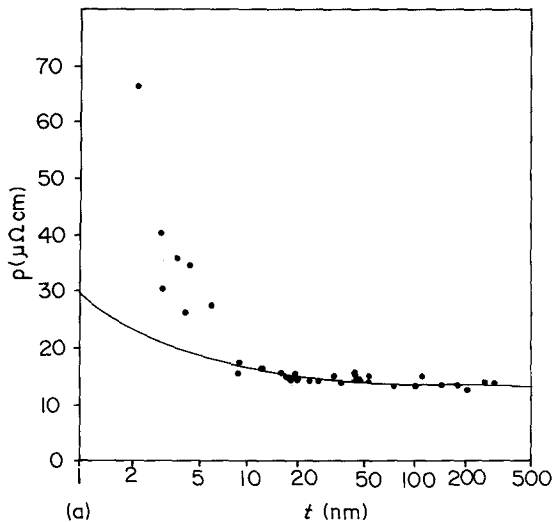

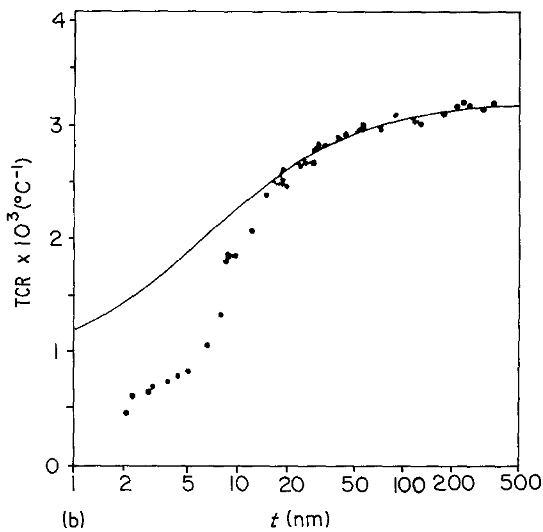

Figure 31 (a) Resistivity against film thickness, (b) TCR against film thickness for platinum films. The solid curves are fitted FS curves (after [243]).

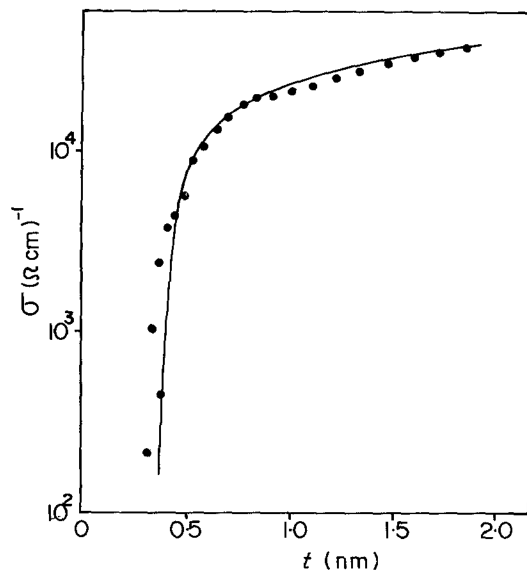

Figure 32 The thickness dependence of the conductivity from measurements (dots) and from fit of Equation 24 with parameters $\sigma_\infty = 5.96 \times 10^4$ $(\Omega\,\text{cm})^{-1}$, $l_0 =$ 11.7 nm, $p = 0.13$ and $h = 0.3$ nm (after [244]).

metal films, the following interesting observations can be made.

1. The transition metal films are generally grown by evaporation on glass substrates.

2. All the transition metal films exhibit a size effect at low thicknesses.

3. With the exception of palladium, the infinitely thick film resistivity (ρ_∞) is considerably higher than the bulk resistivity (ρ_b). This deviation is quite significant for metals with a high melting point. This is generally attributed to the high defect density inherent in thin films.

4. The TCR of transition metal films also exhibit a size effect for lower thicknesses. The TCR is smaller in films compared to bulk crystals. With the exception of yttrium, palladium and platinum, the TCR is negative for ultra-thin films. The TCR is usually negative for very thin films

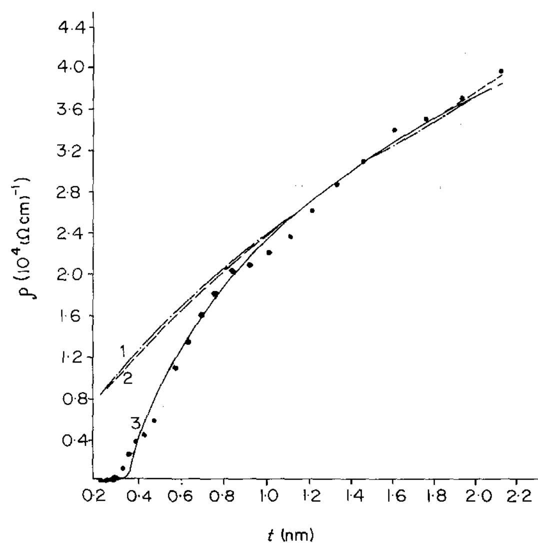

Figure 33 The dependence of the conductivity on the film thickness experimental data. Dots; (1): fitted with FS theory, assuming $p = 0.24$, $\sigma_\infty = 13.8 \times 10^{-6}$ $(\Omega\,\text{cm})^{-1}$ and $l_0 = 20.4$ nm; 2: fitted with FS theory assuming $p = 0$, $\sigma_\infty = 17.2 \times 10^{-4}$ $(\Omega\,\text{cm})^{-1}$ and $l_0 = 18.6$ nm and 3: fitted with the Namba model assuming $p = 0.16$, $\sigma_\infty = 8.85 \times 10^{-4}$ $(\Omega\,\text{cm})^{-1}$, $l_0 = 7.4$ nm and $h = 0.3$ nm (after [244]).

which exhibit a large deviation from ρ_b at higher thicknesses.

5. The reported TEP values on palladium, manganese, chromium and tantalum are in good agreement with the bulk values. The TEP in these films depends on the growth and annealing conditions.

6. In general, electrical resistivity decreases and TCR increases at higher substrate temperature and deposition rate. Film resistivity is usually smaller when grown in UHV conditions compared to the ones deposited in ordinary vacuum ($\sim 10^{-4}$ Pa).

7. Reproducible and reversible experimental results are normally obtained for films annealed at high temperature.

8. In general, films deposited at low substrate temperature (< 80 K) are amorphous while those deposited at high substrate temperature (> 600 K) are monocrystalline.

9. Most authors have used the FS model to analyse their experimental results. FS theory is in good agreement with experimental results at higher thicknesses for $p = 0$, for many transition metal films. More recent experimental reports have also used MS theory to analyse the results. It is rather surprising that no other theoretical models are used to analyse experimental results.

10. Many authors have determined p and l_0 based on FS theory assuming diffuse scattering of carriers. It has been suggested by many authors [230, 231, 245] that it is not possible to determine uniquely l_0, R, p, ρ_∞ using either the FS or MS models in the case of non-monovalent transition metals. The main problem in the evaluation of transport parameters arises in the separation of l_0 and p, and this is not at all possible using the FS model.

11. The agreement between different theoretical models and the experimental data on transition metal films is very satisfactory at higher thicknesses, but in the case of lower thickness films, the deviation is quite significant.

12. It has been suggested [245] that the Namba model, which is an extension of the FS model, can provide a better fit to the experimental results at very low thicknesses and will enable l_0, p, σ_∞ and h to be determined more accurately.

5. Some suggestions for further experimental work on transition metal films

Although there has been remarkable progress during the last couple of decades in accumulating experimental data on the transport properties of transition metal films, further experimentation in this area will certainly enhance our understanding of the complex behaviour of these films. The following are some suggestions for further experimental work on the transport properties of these films.

1. Of the three transport properties reviewed in this article, electrical resistivity and TCR are studied extensively. The TEP is reported for only five transition metal films. It may be still better if all these three transport properties are measured on the same specimen. Chopra [2] has emphasized that the determination of the physical parameters such as electrical resistivity, TCR and TEP becomes meaningful only if all these parameters are measured on the same specimen. No effort has been made in this direction, except for yttrium and palladium.

2. These transport properties are investigated for polycrystalline films and there are very few reports on epitaxial films. It is necessary to perform these experiments on epitaxial films to derive meaningful conclusions from these results.

3. Most of these films are deposited in high vacuum ($\sim 10^{-4}$ Pa), and it is important to grow these films in ultra-high vacuum ($> 10^{-6}$ Pa) and perform these experiments *in situ* to minimize the effect of defects and impurities on the properties of thin films.

4. There are very few reports on the effect of deposition parameters on these transport properties of many transition metal films. Deposition parameters such as substrate temperature, pressure, evaporation rate and substrate material have a strong influence on the transport properties of films.

5. The critical value of the T_s responsible for the epitaxial growth of films also depends on the nature of substrate, vacuum and deposition rate. Although there are many reports about this on semiconductor films, the available experimental data regarding this important and useful information on transition metal films are not exhaustive.

6. Systematic studies on the structural aspect of thin films by electron microscope will certainly aid in the proper interpretation of the experimental results.

7. To the best of the author's knowledge, the transport properties of technetium (Tc), ruthenium

(Ru), iridium (Ir) and osmium (Os) are not reported so far.

6. Conclusions

The experimental results on the transport properties of nineteen transition metal films have been reviewed. Most of these films deposited by evaporation in high-vacuum are polycrystalline. In general, the deposition parameters play a crucial role in determining thin film properties. Thus, by a proper choice of the evaporating and measuring conditions, film properties can be controlled. This information will be very useful in the fabrication of thin film devices. An attempt has been made to review all the theoretical models published so far on electrical resistivity, TCR and TEP of thin metal films. Theoretical models to analyse experimental results in discontinuous metal films are far from satisfactory. It may be necessary to develop more general theoretical models which can account for any variation in the film conductivity due to the changes in the deposition conditions. A careful structural study on discontinuous and continuous metal films may provide a deeper insight into the conduction mechanism of thin films. It may be possible to understand the complex behaviour of the transport properties of these transition metal films if appropriate theoretical models are used to analyse the experimental results. More experimental measurements on transition metal films deposited under UHV conditions and studied in monocrystalline form, at low temperature, will definitely enhance our knowledge of the electronic structure of these interesting and useful materials.

Acknowledgements

The author is grateful to the British Library, Lending Division, UK for providing promptly the photocopies of many research papers referred to in this article. The author is also grateful to the staff of the Central Library, University of the West Indies, for providing the necessary research material to prepare this review article. The author is grateful to Dr R. Whiting and Dr A. Tang-Kai for many useful comments on the manuscript.

References

1. L. I. MAISSEL, "Handbook of Thin Film Technology", edited by L. I. Maissel and R. Glang (McGraw-Hill, New York, 1970) Chap. 13.
2. K. L. CHOPRA, "Thin Film Phenomena" (McGraw-Hill, New York, 1970).
3. D. C. LARSON, "Physics of Thin Films", Vol. 6, edited by M. H. Francombe and R. W. Hoffmann (Academic Press, New York, 1971).
4. R. M. HILL, *Thin Solid Films* **12** (1972) 367.
5. M. R. BENNETT and J. G. WRIGHT, *Phys. Status Solidi* **13(a)** (1972) 135.
6. P. N. BAKER, *Thin Solid Films* **14** (1972) 3.
7. R. H. BUBE, *Ann. Rev. Mater. Sci.* **5** (1975) 201.
8. P. G. BORZIAK and Yu. A. KULYUPIN, *Thin Solid Films* **44** (1977) 1.
9. T. J. COUTTS, "Active and Passive Thin Film Devices", edited by T. J. Coutts (Academic Press, New York, 1978) Chapts. 3 and 5.
10. A. SOMMERFELD, *Z. Physik* **47** (1928) 1.
11. J. M. ZIMAN, "Electrons and Phonons" (Oxford University Press, London, 1962) pp. 486–490.
12. R. F. GREENE, *J. Phys. Chem. Solids* **14** (1960) 291.
13. *Idem, Surface Sci.* **2** (1964) 101.
14. C. A. NEUGEBAUER and R. H. WILSON, "Basic Problems in Thin Film Physics" (Vandenhock and Rupprecht, Gottingen, 1966) p. 579.
15. N. MOSTOVETCH and B. VODAR, "Semiconducting Materials", edited by H. K. Henisch (Butterworth, London, 1951) pp. 260–81.
16. N. NIFONTOFF, *C. R. Acad. Sci. Paris* **236** (1953) 538, 2486; *ibid.* **237** (1953) 24.
17. K. Van STEENSEL, *Philips Res. Repts.* **22** (1967) 246.
18. C. A. NEUGEBAUER and M. B. WEBB, *J. Appl. Phys.* **33** (1962) 74.
19. T. E. HARTMAN, *ibid.* **34** (1963) 943.
20. R. M. HILL, *Thin Solid Films* **1** (1967) 39.
21. N. F. MOTT, *Phil. Mag.* **19** (1969) 835.
22. P. SHENG, B. ABELES and Y. ARIE, *Phys. Rev. Lett.* **31** (1973) 44.
23. J. BERNASCONI, *Phys. Rev. B* **7** (1973) 2252.
24. R. M. HILL and T. J. COUTTS, *Thin Solid Films* **42** (1977) 201.
25. C. J. ADKINS, *J. Phys. C (Solid State)*, in press.
26. T. G. ANDERSON and S. H. NORRMANN, *Phys. Status Solidi* **62(a)** (1980) K127.
27. S. H. NORRMAN and T. G. ANDERSON, *J. Appl. Phys.* **52** (1981) 6673.
28. J. J. THOMSON, *Proc. Camb. Phil. Soc.* **11** (1901) 120.
29. K. FUCHS, *ibid.* **34** (1938) 100.
30. T. J. COUTTS, "Electrical Conduction in Thin Metal Films" (Elsevier Scientific Pub. Co., Amsterdam, 1976) p. 162.
31. E. H. SONDHEIMER, *Adv. Phys.* **1** (1952) 1.
32. D. S. CAMPBELL, "The Use of Thin Films in Physical Investigations", edited by J. C. Anderson (Academic Press, New York, 1966).
33. J. BORRAJO and J. M. HERAS, *Thin Solid Films*, **18** (1973) 267.
34. P. A. KRISHNAMURTHY and G. K. SHIVAKUMAR, *J. Mater. Sci. Lett.* **1** (1982) 453.
35. G. C. JAIN and B. S. VERMA, *Thin Solid Films* **15** (1967) 156.
36. D. DESCHACHT, A. BOYER and E. GROUBERT, *ibid.* **70** (1980) 311.

37. IJAZ-UR-RAHAMAN, *J. Appl. Phys.* **52** (1981) 5859.
38. M. S. P. LUCAS, *ibid.* **36** (1965) 1632.
39. J. E. PARROT, *Proc. Phys. Soc. (London)* **85** (1975) 1143.
40. G. BRÄNDLI and P. COTTI, *Helv. Phys. Acta* **38** (1965) 801.
41. R. ENGLEMAN and E. H. SONDHEIMER, *Proc. Phil. Soc.* **69** (1956) 449.
42. S. B. SOFFER, *J. Appl. Phys.* **38** (1967) 1710.
43. M. GRENDEL, Thesis, Faculty of Science, Department of General Physics, Bratislava (1979).
44. A. M. GHODGAONKAR and A. D. TILLU, *J. Phys. D (Appl. Phys.)* **10** (1977) 1329.
45. A. M. GHODGAONKAR and K. RAMANI, *J. Appl. Phys.* **52** (1981) 4869.
46. G. WEDLER, F. J. BROCKER, H. G. KOCK and C. WOLFING, Proceedings of International Symposium, Clausthal-Gottingen, edited by R. Niedermer and H. Mayer, (1966) p. 566.
47. Y. NAMBA, *Jpn. J. Appl. Phys.* **9** (1970) 1326.
48. K. C. ELSON and J. SAMBLES, *J. Phys. F (Met. Phys.)* **11** (1981) 647.
49. A. A. COTTEY, *Thin Solid Films* **1** (1967/1968) 297.
50. C. R. TELLIER, C. R. PICHARD and A. J. TOSSER, *J. Mater. Sci. Lett.* **1** (1982) 271.
51. A. F. MAYADAS and M. SHATZKES, *Phys. Rev. B* **1** (1970) 1382.
52. A. F. MAYADAS, M. SHATZKES and J. F. JANAK, *Appl. Phys. Lett.* **14** (1969) 345.
53. E. E. MOLA and J. M. HERAS, *Electrocompon. Sci. Technol. (GB)* **1** (1974) 77.
54. C. R. TELLIER, C. R. PICHARD and A. J. TOSSER, *J. Phys. F (Met. Phys.)* **9** (1979) 2377.
55. C. R. TELLIER and A. J. TOSSER, *Appl. Phys.* **14** (1977) 221; *Thin Solid Films* **43** (1977) 261; *ibid.* **44** (1977) 141.
56. C. R. TELLIER, *ibid.* **51** (1978) 311.
57. P. WISSMANN, *ibid.* **5** (1970) 329.
58. G. WEDLER and P. WISSMAN, *Ber. Bunsenges. Phys. Chem.* **74** (1970) 934.
59. F. THIEME and W. KIRSTEIN, *Thin Solid Films* **30** (1975) 371.
60. C. R. TELLIER, C. R. PICHARD and A. J. TOSSER, *ibid.* **76** (1981) 129.
61. L. A. FALKOVSKY, *J. Exptl. Theoret. Phys.* **64** (1973) 1855.
62. A. M. GHODGAONKAR and K. RAMANI, *Phys. Status. Solidi* **73(a)** (1982) K21.
63. C. R. PICHARD, C. R. TELLIER and A. J. TOSSER, *J. Phys. D (Appl. Phys.)* **12** (1979) L101.
64. A. R. VAMADATT, *Ind. J. Pure Appl. Phys.* **10** (1972) 842.
65. C. R. TELLIER and A. J. TOSSER, *Thin Solid Films* **44** (1977) 141.
66. B. S. VERMA and S. K. SHARMA, *ibid.* **5** (1970) R44.
67. P. M. HALL, *Appl. Phys. Lett.* **12** (1968) 212.
68. F. WARKUSZ, *J. Phys. D (Appl. Phys.)* **11** (1978) 689.
69. H. HELMS and A. SCHEIBE, *Thin Solid Films* **78** (1981) L49.
70. N. JAIN and R. SRIVASTAVA, *J. Mater. Sci. Lett.* **1** (1982) 330.
71. C. R. TELLIER and A. J. TOSSER, *Thin Solid Films* **52** (1978) 53.
72. *Idem, ibid.* **42** (1977) L31.
73. *Idem, ibid.* **41** (1977) 161.
74. C. R. TELLIER, A. J. TOSSER and L. HAFID, *J. Mater. Sci.* **15** (1980) 2875.
75. C. R. TELLIER, C. R. PICHARD and A. J. TOSSER, *ibid.* **17** (1982) 290.
76. C. R. PICHARD, A. J. TOSSER and C. R. TELLIER, *ibid.* **17** (1982) 10.
77. F. WARKUSZ, *Thin Solid Films* **52** (1978) L9.
78. C. R. PICHARD, C. R. TELLIER, L. OUARBYA and A. J. TOSSER, *Phys. Status Solidi* **68(a)** (1981) 477.
79. B. S. VERMA and G. C. JAIN, *Thin Solid Films* **10** (1972) 71.
80. F. WARKUSZ, *Electrocomp. Sci. Technol.* **5** (1978) 197.
81. *Idem, Acta Phys. Polon.* **A54** (1978) 31.
82. C. R. TELLIER and A. J. TOSSER, *Electrocomp. Sci. Technol.* **6** (1979) 37.
83. C. R. PICHARD, A. J. TOSSER and C. R. TELLIER, *ibid.* **6** (1980) 87.
84. C. R. TELLIER, C. R. PICHARD and A. J. TOSSER, *Thin Solid Films* **61** (1979) 349.
85. C. R. PICHARD, C. R. TELLIER and A. J. TOSSER, *ibid.* **62** (1979) 189.
86. V. B. LOBODA and I. E. PROTSENKO, *Cryst. Res. Technol. (Germany)* **16** (1981) 489; *ibid.* **16** (1981) 357.
87. V. B. LOBODA, I. E. PROTSENKO and V. G. SHAMONYA, *Ukr. Fiz. Zh.* **27** (1982) 1343.
88. V. B. LOBODA, I. E. PROTSENKO and A. V. YAREMENKO, *Krist. Tech. (Germany)* **15** (1983) 43.
89. A. E. CURZON and O. SINGH, *Thin Solid Films* **57** (1979) 157; *J. Phys. F (Met. Phys.)* **8** (1978) 1619.
90. V. N. KOUL and O. N. SRIVASTAVA, *J. Less-common Met.* **57** (1978) 221.
91. M. A. ANGADI and P. V. ASHRIT, *ibid.* **75** (1980) 147.
92. *Idem, Thin Solid Films* **72** (1980) L5.
93. *Idem, J. Mater. Sci.* **18** (1983) 3177.
94. R. CHANDER, R. E. HOWARD and S. C. JAIN, *Ind. J. Pure Appl. Phys.* **5** (1967) 397.
95. P. E. FRIEBERTSHAUSER and J. W. McCAMONT, *J. Vac. Sci. Technol.* **6** (1969) 184.
96. F. F. WAWNER Jr and K. R. LAWLESS, *ibid.* **6** (1969) 588.
97. E. GRUNBAUM and R. SCHWARZ, *J. Appl. Phys.* **40** (1969) 3364.
98. V. G. PYNKO, L. I. KVEGLIS and V. S. KORCHMAR, *Fiz. Tver. Tela* **13** (1971) 3334.
99. A. HOLZ and G. GOULD, *Thin Solid Films* **14** (1972) 35.
100. G. GOULD, C. GRAHAM, E. GRUNBAUM, L. MORAGA, J. MÜLLER and D. C. LARSON, *ibid.* **13** (1972) 61.
101. B. SINGH and N. A. SURPLICE, *ibid.* **10** (1972) 243.
102. O. TSUKIDE, M. YAMASHITA and S. ANDO, *J.*

Vac. Soc. Jpn. **18** (1975) 306.
103. Y. IGASAKI and H. MITSUHASHI, *Thin Solid Films* **51** (1978) 33.
104. B. L. MEL'NICHUK and Z. V. STASYUK, *Fiz. Met. Metalloved.* **46** (1978) 1115.
105. M. T. THOMAS, *J. Electrochem. Soc. (USA)* **117** (1970) 396.
106. F. T. J. SMITH, *J. Appl. Phys.* **41** (1970) 4227.
107. T. NAKAMURA, T. GOTO and S. YAMANAKA, *Oyo Buturi (Japan)* **44** (1975) 231.
108. R. RADEBANCK and P. H. KEESOM, *Phys. Rev.* **149** (1966) 217.
109. R. CHANDER, R. E. HOWARD and S. C. JAIN, *J. Appl. Phys.* **38** (1967) 4092.
110. R. CHANDER and S. C. JAIN, *ibid.* **39** (1968) 5343.
111. S. C. JAIN and R. CHANDER, *Thin Solid Films* **4** (1969) R11.
112. C. REALE, *Phys. Status Solidi* **58(b)** (1973) K5.
113. N. E. ALEKSEEVSKII, V. M. SAKOSARENKO, K. BLUTHNER and H. J. KOHLER, *Phys. Status Solidi* **34(a)** (1976) 541.
114. N. A. CHERNOPLEKOV, G. H. PANOVA, B. N. SAMOILOV and A. A. SHIKOV, *Zh. Eksp. Teor. Fiz.* **64** (1973) 195.
115. R. J. NÖER, *Phys. Rev. B* **12** (1975) 4882.
116. A. BORODZIUK-KULPA, B. STOLECKI and C. WESOLOWSKA, *Thin Solid Films* **67** (1980) 21.
117. *Idem, ibid.* **85** (1981) 323.
118. *Idem, J. Mater. Sci.* **16** (1981) 1661.
119. J. R. RAIRDEN and J. FUREY, US Patent, 3 432 416 (1966).
120. J. SOSNIAK, *J. Appl. Phys.* **39** (1968) 4157.
121. S. OGAWA, T. YOTSUYA and T. HASEGAWA, *Thin Solid Films* **36** (1976) 59.
122. K. REICHE and G. POMPE, *J. Low. Temp. Phys.* **36** (1979) 467.
123. R. M. CHAPMAN, *Vacuum* **13** (1963) 213.
124. P. N. DENBIGH and R. B. MARCUS, *J. Appl. Phys.* **37** (1966) 4325.
125. E. KRIKORIAN and R. J. SNEED, *ibid.* **37** (1966) 3674.
126. W. T. LAYTON and H. E. CULVER, Proceedings of Electronic Components Conference (1966) p. 225.
127. J. DESSERRE and J.-C. GOULET, *C. R. Hebd. Sean. Acad. Sci. B (France)* **272** (1971) 808.
128. W. R. HARDY and J. SHEWCHUM, *Thin Solid Films* **8** (1971) 81.
129. D. J. WILLMOTT, *J. Appl. Phys.* **43** (1972) 4865.
130. A. SCHAUER and M. ROSCHY, *Thin Solid Films* **12** (1972) 313.
131. Ya. S. UMANSKII, U. S. URAZALIEV and R. D. IVANOV, *Fiz. Met. Metalloved.* **33** (1972) 196.
132. N. WATERHOUSE, P. S. WILCOX and D. J. WILLMOTT, *J. Appl. Phys.* **42** (1971) 5649.
133. N. WATERHOUSE, *ibid.* **43** (1972) 1498.
134. L. G. FEINSTEIN and D. GERSTENBERG, *J. Vac. Sci. Technol.* 9 (1972) 445.
135. J. RACHMAN and W. JUERGENS, *Thin Solid Films,* **26** (1975) 305.
136. A. PERINATI and G. F. PIACENTINI, *J. Vac. Sci. Technol.* **14** (1977) 169.
137. T. SHIOYAMA, S. OGAWA and K. YAMANAKA, *Thin Solid Films* **58** (1979) 127.
138. F. BRIONES and D. GOLMAYO, *ibid.* **57** (1979) 332.
139. D. M. HOFFMAN and J. RISEMAN, Transactions of 4th National Vacuum Symposium (1957) p. 42; Transaction of 7th National Vacuum Symposium (1960) p. 218.
140. K. B. SCOW and R. E. THUN, Transaction of 9th National Vacuum Symposium (1962) p. 151.
141. P. A. GOULD, *Brit. J. Appl. Phys.* **16** (1967) 1481.
142. S. FUJIME, *Jpn. J. Appl. Phys.* **5** (1966) 1029.
143. CHIN-SHUN LU and A. A. MILGRAM, *J. Vac. Sci. Technol.* **4** (1967) 49; *J. Appl. Phys.* **39** (1968) 1624.
144. V. G. PERMYAKOV and Ya. N. PROLEEVA, *Izv. VUZ. Fiz.* **56** (1971) 121.
145. G. J. CHASSAING and M. L. SIGRIST, *Thin Solid Films* **16** (1973) 37.
146. K. HIEBER and L. LASSAK, *ibid.* **20** (1974) 63.
147. B. W. LICZNERSKI, *ibid.* **36** (1976) 61.
148. H. SANCHEZ, E. POSADA, J. PANQUEVA, E. PAEZ, I. JARAMILLO and G. FRITSCH, *Vacuum* **27** (1977) 163.
149. L. A. UDACHAN, S. M. SHIVAPRASAD, P. V. ASHRIT and M. A. ANGADI, *Phys. Status Solidi* **60(a)** (1980) K191.
150. T. IMURA, *Jpn. J. Appl. Phys.* **19** (1980) 215.
151. M. A. ANGADI and L. A. UDACHAN, *J. Mater. Sci.* **16** (1981) 1412.
152. B. I. BELEVTSEV, Yu. F. KOMNIK and L. A. YATSUK, *Fiz. Nizk. Temp.* **8** (1982) 1065.
153. M. A. ANGADI and L. A. UDACHAN, *J. Mater. Sci. Lett.* **1** (1982) 539.
154. *Idem, ibid.* **2** (1983) 379.
155. *Idem, ibid.* Submitted for publication.
156. T. IMURA, *Thin Solid Films* **94** (1982) 249.
157. M. V. VEDERNIKOV, *Adv. Phys.* **16** (1969) 337.
158. H. J. DEGENHART, Proceedings of Electronic Components Conference (1967) p. 84.
159. F. M. d'HEURLE, *Trans. Metall. Soc. AMIE* **236** (1966) 321.
160. P. E. FRIEBERTHAUSER, *J. Vac. Sci. Technol.* **7** (1970) 485.
161. H. OIKAWA, *ibid.* **15** (1978) 1117.
162. K. UDA, Y. MATSUSHITA and S. TAKASU, *J. Appl. Phys.* **51** (1980) 1039.
163. J. NAGANO, *Thin Solid Films* **67** (1980) 1.
164. I. VAVRA and S. LUBY, *ibid.* **69** (1980) 169.
165. A. SINGH, *J. Inst. Electron Telecommun. Eng. (India)* **26** (1980) 299.
166. E. R. BOWERMAN, J. W. CULP, E. F. HUDOCK, F. LEDER and H. J. DEGENHART, Proceedings of Electronic Components Conference (1963) p. 158.
167. K. L. CHOPRA, M. R. RANDLETT and R. H. DUFF, *Appl. Phys. Lett.* **9** (1966) 402.
168. P. J. DOBSON and B. J. HOPKINS, *J. Appl. Phys.* **39** (1968) 3074.
169. T. T. SHENG, R. B. MARCUS, F. ALEXANDER and W. A. REED, *Thin Solid Films* **14** (1972) 289.
170. P. M. PETROFF and W. A. REED, *ibid.* **21** (1974) 73.
171. P. Yu. YAROSHEVICH, *Fiz. Met. Metalloved. (USSR)* **40** (1975) 1308.

172. A. D. C. GRASSIE and K. G. ADANU, *Solid State Commun.* **24** (1977) 345.
173. A. D. C. GRASSIE and F. BOAKYE, *Thin Solid Films* **57** (1979) 169.
174. E. M. CASTRO and J. BEYNON, *ibid.* **69** (1980) L43.
175. A. A. SAWICKI and J. BEYNON, *ibid.* **70** (1980) L21.
176. E. M. CASTRO and J. BEYNON, *ibid.* **69** (1980) L21.
177. M. A. ANGADI and S. M. SHIVAPRASAD, *J. Phys. D (Appl. Phys.)* **13** (1980) L157.
178. *Idem, Thin Solid Films* **71** (1980) L1.
179. M. A. ANGADI, S. M. SHIVAPRASAD and P. V. ASHRIT, *Phys. Status Solidi* **60(a)** (1980) K159.
180. M. A. ANGADI and S. M. SHIVAPRASAD, *J. Phys. D (Appl. Phys.)* **14** (1981) 1125.
181. *Idem, J. Mater. Sci. Lett.* **2** (1983) 207.
182. *Idem, ibid.* **3** (1984) 739.
183. F. J. HEMMER, C. FELDMAN and W. T. LAYTON, Proceedings of National Electronic Conference **20** (1964) 201.
184. D. D. ZIMMERMAN, Proceedings of Microelectronics Symposium (1965) 2C-7.
185. P. E. FRIEBERTHAUSER and H. A. NOTARYS, *J. Vac. Sci. Technol.* **7** (1970) 485.
186. V. P. DIMITRIEV, A. K. MILAI and A. F. ORLOV, *Sov. J. Low Temp. Phys.* **1** (1975) 438.
187. A. UL. HAQ and O. MEYER, *Thin Solid Films,* **94** (1982) 119.
188. D. M. HOFFMAN and M. D. COUTTS, *J. Vac. Sci. Technol.* **13** (1976) 122.
189. J. KOSHY, *J. Phys. D (Appl. Phys.)* **13** (1980) 1339.
190. E. F. WASSERMAN and W. SANDER, *ibid.* **6** (1969) 537.
191. F. J. KOLLARITS and R. SPEISER, *Thin Solid Films* **35** (1976) 131.
192. S. J. RAEBURN and R. V. ALDRIDGE, *Phys. Lett.* **A66** (1978) 311; *J. Phys. F (Met. Phys.)* 8 (1978) 1917.
193. R. BLANC, C. CAMOIN, H. AKHOUAIRY, M. BELZONS and N. RIVIER, *Solid State Commun.* **33** (1980) 517.
194. T. YOSHIE, K. YAMAKAWA and F. E. FUJITA, *J. Phys. Soc. Jpn.* **37** (1974) 572.
195. F. SAVORNIN, *Ann. Phys.* **5** (1960) 1355.
196. J. BORRAJO and J. M. HERAS, *Surface Sci.* **28** (1971) 132; *Thin Solid Films* **18** (1973) 267.
197. E. E. MOLA, J. BORRAJO and J. M. HERAS, *ibid.* **34** (1973) 561.
198. R. D. FISHER and S. D. TAYLER, *J. Appl. Phys.* **37** (1966) 2512.
199. J. KATO and S. OGAWA, *Jpn. J. Appl. Phys.* **9** (1970) 875.
200. D. WATANABE and R. MIIDA, *ibid.* **11** (1972) 296.
201. G. J. Van GURP, *J. Appl. Phys.* **46** (1975) 1922; *J. Phys. Chem. Solids* **38** (1977) 627.
202. A. K. PAL, S. CHAUDHURI and A. K. BARUA, *J. Phys. D (Appl. Phys.)* **9** (1976) 2261.
203. M. M. L. KWAN and R. W. HOFFMAN, *Jpn. J. Appl. Phys.* **1** (1974) 279.
204. P. WHYMAN and R. V. ALDRIDGE, *J. Phys. F (Met. Phys.)* **4** (1974) L6.
205. C. REALE, *Electron. Compon. (GB)* **9** (1968) 288; *Phys. Lett.* **A24** (1967) 145.
206. N. A. MIKOLAICHUK, R. S. PANCHISHIN and Z. V. STASYUK, *Ukrayin. Fiz. Zh.* **14** (1969) 741.
207. J. Le BAS, *C. R. Acad. Sci. B (France)* **268** (1969) 1393.
208. J. KLEEFELD and A. A. HIRSCH, *Vacuum* **19** (1969) 561.
209. B. S. VERMA, *Ind. J. Pure Appl. Phys.* **9** (1971) 237.
210. G. WEDLER, H. REICHENBERGER and H. WENZEL, *Z. Naturforsch.* **26A** (1971) 1444.
211. H. REICHENBERGER, G. WEDLER, H. WENZEL and C. WOLFING, *Ber. Bunsenges. Phys. Chem.* **75** (1971) 1033.
212. A. LAL and V. P. DUGGAL, *Thin Solid Films* **14** (1972) 373.
213. S. CHAUDHURI, A. K. PAL and A. K. BARUA, *J. Appl. Phys.* **46** (1975) 3465.
214. M. TAKASHAHI and T. SUZUKI, *Jpn. J. Appl. Phys.* **16** (1977) 2271.
215. H. LUTZ, P. SCHOBORIA, J. E. CROW and T. MIHALISIN, *Phys. Rev. B* **18** (1978) 3600.
216. A. H. EID, S. MAHMOUD, M. S. ELMANHARAWY and S. T. BADAR, *Czech. J. Phys.* **B29** (1979) 451.
217. C. K. GHOSH and A. K. PAL, *J. Appl. Phys.* **51** (1980) 2281.
218. V. STARY and K. SEFCIK, *Vacuum,* **31** (1981) 345.
219. M. A. ANGADI and L. A. UDACHAN, *Thin Solid Films* **79** (1981) 149.
220. G. WEDLER and W. DRAXLER, *Int. J. Quant. Chem.* **19** (1981) 1027.
221. C. REALE, *J. Less-common Met.* **18** (1969) 167.
222. O. N. SRIVASTAVA, *Thin Solid Films* **3** (1969) 127.
223. L. E. MURR and G. WONG, Proceedings of the 28th Annual Meeting of Electron Microscopy Society of America, Baton Rouge, USA (Claitor's Pub. Div. 1970) p. 456.
224. D. W. STOPS, *Thin Solid Films* **41** (1977) 149.
225. A. BARR, *ibid.* **41** (1977) 217.
226. F. ANTONANGELI, A. BALZAROTTI, A. BIANCONI, E. BURATTINI and P. PERFETTI, *Phys. Status Solidi* **42(a)** 1977 K41.
227. M. A. ANGADI, S. M. SHIVAPRASAD and L. A. UDACHAN, *Phys. Lett.* **A78** (1980) 187.
228. M. A. ANGADI and S. M. SHIVAPRASAD, *J. Phys. D (Appl. Phys.)* **13** (1980) L171.
229. D. STARK and P. ZWICKNGL, *Appl. Phys. (Germany),* **21** (1980) 397.
230. G. WEDLER and G. ALSHORACHI, *Thin Solid Films,* **74** (1980) 1.
231. G. WEDLER and R. CHANDER, *ibid.* **65** (1980) 53.
232. M. A. ANGADI and S. M. SHIVAPRASAD, *Vacuum* **32** (1982) 51.
233. *Idem, J. Mater. Sci. Lett.* **1** (1982) 65.
234. K. B. SINGH and J. HATIBARUA, *Ind. J. Pure Appl. Phys.* **20** (1982) 183.
235. M. A. ANGADI and S. M. SHIVAPRASAD, *J. Mater. Sci. Lett.* **2** (1983) 207.
236. *Idem, J. Mater. Sci.* **19** (1984) 2396.
237. M. J. BURNS, W. C. McGINNIS, R. W. SIMON, G. DEUTSCHER and P. M. CHAIKIN, *Phys. Rev. Lett.* **47** (1981) 1620.

238. E. ABRAHAMS, P. W. ANDERSON, D. C. LICCIARDELLO and T. V. RAMAKRISHNAN, *ibid.* **42** (1979) 673.
239. J. JAUNET, P. HAYMANN and A. ART, *C. R. Acad. Sci. B (France)* **265** (1967) 329.
240. K. MISEK, *Czech. J. Phys.* **B20** (1970) 1214.
241. C. REALE, *ibid.* **B21** (1971) 662.
242. J. M. HERAS, *Thin Films* **2** (1971) 25; 39.
243. H. HOFFMANN and G. FISCHER, *Thin Solid Films* **36** (1976) 25.
244. G. FISCHER, H. HOFFMANN and J. VANCEA, *Phys. Rev. B* **22** (1980) 6065.
245. H. HOFFMAN and J. VANCEA, *Thin Solid Films* **85** (1981) 147.

Received 14 March
and accepted 12 April 1984